

Plasmonics of non-noble metals

Michal Horák,^{*,†} Michael Foltýn,[†] Viktor Bajo,^{†,‡} Petr Dub,^{†,‡} and Tomáš

Šikola^{†,‡}

[†]*Brno University of Technology, Central European Institute of Technology, Purkyňova 123,
612 00, Brno, Czech Republic*

[‡]*Brno University of Technology, Faculty of Mechanical Engineering, Institute of Physical
Engineering, Technická 2, 616 69, Brno, Czech Republic*

E-mail: michal.horak2@ceitec.vutbr.cz

Abstract

Localized surface plasmon resonances are self-sustained, collective oscillations of free electrons in metallic nanostructures. They have a wide range of applications. The most common plasmonic metals are noble metals, such as gold and silver. However, there are applications, such as surface-enhanced Raman spectroscopy, in which using non-noble metals is advantageous. This review summarizes the investigation of localized surface plasmons in non-noble metal nanoparticles, providing an overview of the plasmonic properties of non-noble metals. We cover the following metals: aluminium (Al), antimony (Sb), bismuth (Bi), chromium (Cr), copper (Cu), gallium (Ga), indium (In), lead (Pb), magnesium (Mg), molybdenum (Mo), nickel (Ni), potassium (K), selenium (Se), sodium (Na), tellurium (Te), tin (Sn), titanium (Ti), tungsten (W), and zinc (Zn). Our summary therefore compares the plasmonic properties of non-noble metals and briefly introduces their potential to the readers.

Introduction

The interaction of the electromagnetic field and free electrons in metals at the metal-dielectric interface gives rise to hybrid light-matter states called surface plasmon polaritons (SPPs). Their generation and propagation are studied by a branch of nanooptics called plasmonics. It is often sufficient to view the SPPs as an evanescent electromagnetic wave propagating along the metal-dielectric interface and exponentially decaying in the direction perpendicular to the interface. In metallic nanostructures, collective oscillations of free electrons strongly couple to the electromagnetic field forming the excitations called localized surface plasmon resonances (LSPRs).¹ The clear mathematical foundation for LSPRs was established by Gustav Mie in 1908.² Their characteristic feature is a strong enhancement of the electromagnetic field within the surrounding dielectric together with its confinement on the subwavelength scale, which can be utilized to control various optical processes in a wide spectral region even below the free space diffraction limit.^{3,4} The significance of this feature is further in-

creased by the easy tunability of the optical properties of nanostructures by engineering their size, shape, or dielectric environment.⁵ This flexibility in design allows one to create a large amount of optical functions. Therefore, plasmonic nanostructures have a wide field of applications,⁶ including photonics,⁷ microscopy,⁸ spectroscopy,⁹ energy harvesting,¹⁰ medicine,¹¹ sensing,^{12,13} and catalysis.^{14–16}

New discoveries with high application potential are often connected to the implementation of new concepts in the field of plasmonics, such as a plasmoelectric effect,¹⁷ plasmonic lasing,¹⁸ generalized laws of reflection,¹⁹ spin-orbit coupling,²⁰ chirality,²¹ or Babinet’s principle of complementarity.^{22–24} In addition, unconventional plasmonic materials are utilized in specific application fields, including the prospect of spectro-electrochemistry of silver amalgam nanoparticles²⁵ or tunable plasmonic devices or metasurfaces made of phase-changing materials such as vanadium dioxide^{26–29} or gallium.^{30–32} Additionally, the native oxide layer on non-noble metallic nanostructures can suppress the catalytic activity of the nanoparticles similarly to the activity achieved by covering gold nanoislands with a graphene cover layer³³ or by shell-isolated nanoparticles.³⁴

The most common plasmonic metals are gold, silver, and to a lesser extent aluminium. They were found to be ideal plasmonic materials for their availability, relative chemical stability, nontoxicity, and ease of production in the industry. The only issue regarding aluminium and silver is the instability of antennas due to oxidation, which with time changes the structure and, with it, the plasmonic behavior. Furthermore, these metals (except aluminium) can be used for plasmonic applications only in the visible and near-infrared parts of the spectrum,³⁵ as their performance is restricted at lower wavelengths by interband transitions. Consequently, gold supports LSPR at wavelengths longer than 550 nm and silver supports LSPR above 350 nm. Therefore, it is vital to explore other plasmonic materials, which can be used in visible to near-ultraviolet spectral region. Metals are generally considered good plasmonic materials in a certain spectral region if their real part of the dielectric function is negative and their imaginary part of the dielectric function, related to the losses,

is small enough. The ultraviolet and whole visible spectral range is covered by aluminium,³⁶ bismuth,^{37,38} gallium,^{39–41} magnesium⁴² and silver amalgam.²⁵ The ultraviolet plasmonic activity for chromium, copper, indium, lead, palladium, platinum, rhodium, ruthenium, tellurium, tin, titanium and tungsten was also theoretically studied and discussed.^{35,43,44} The aim of this review is to summarize the knowledge in the field of plasmonics of non-noble metals and inspire future investigations in this field.

Noble and non-noble metals

A noble metal is a metallic chemical element that is generally resistant to corrosion and oxidation, even at high temperatures. It is usually found in nature in its raw form. The most common noble metals include gold (Au), silver (Ag), and platinum group metals: platinum (Pt), palladium (Pd), rhodium (Rh), ruthenium (Ru), osmium (Os), and iridium (Ir). In more specialized fields of applications, the number of elements counted as noble metals can be smaller or larger. However, we will follow this division. Plasmonic activity for all noble metals has been explored, including osmium⁴⁵ and iridium^{46,47} that have not been mentioned in the Introduction.

Non-noble metals are metals that are generally not resistant to corrosion and oxidation, especially in moist or acidic environments. They tend to react more easily with other substances, such as oxygen or acids, compared to noble metals, which are more stable and inert. In this review, we focus on non-noble metals, i.e., all metals that are not listed above in the list of noble metals. The following non-noble metals were studied and discussed: aluminium (Al), antimony (Sb), bismuth (Bi), chromium (Cr), copper (Cu), gallium (Ga), indium (In), lead (Pb), magnesium (Mg), molybdenum (Mo), nickel (Ni), potassium (K), selenium (Se), sodium (Na), tellurium (Te), tin (Sn), titanium (Ti), tungsten (W), and zinc (Zn). In the following, we summarize the research in the field of plasmonic properties of these non-noble metals in detail. Figure 1 shows a periodic table with marked noble and non-noble metals

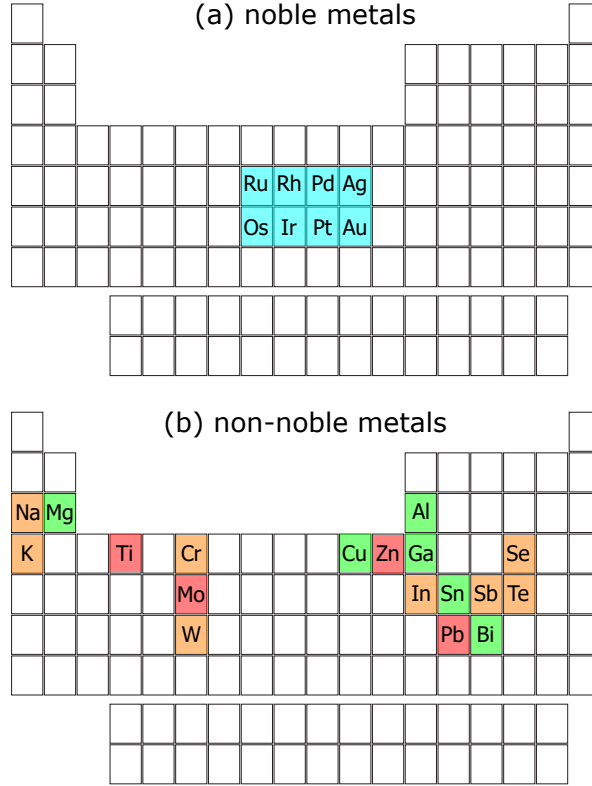


Figure 1: Noble (a) and non-noble (b) metals used in plasmonic applications. In the following, we focus mostly of the non-noble metals marked by green color as they are commonly used in plasmonic applications, whereas the non-noble metals marked by orange color are less employed in plasmonic applications. In addition, plasmonic activity of non-noble metals marked by red color was just predicted with no reported experimental applications.

used in plasmonic applications.

The following discussion focuses on an overview of the investigations of the plasmonic properties of non-noble metal nanostructures, as well as the key parameters for plasmonics, such as their experimental dielectric functions (some of them were obtained using Refractiveindex.info⁴⁸), the theoretical quality factor of LSPR considering the figure of merit derived from the dielectric function as $Q_{\text{LSPR}} = -\Re(\epsilon)/\Im(\epsilon)$, and the Fröhlich energy, i.e. the energy at which the Fröhlich condition is fulfilled.³⁵ It is important to note that the Fröhlich condition is the condition for LSPR in metallic spherical nanoparticles much smaller than the wavelength of light embedded in a homogeneous medium. This condition is derived from the electrostatic approximation of the Mie theory when the denominator of the polarizability

Table 1: Fröhlich energy of selected non-noble metals

material	E_F [eV]	dielectric function reference
Al	8.9	Rakić ⁴⁹
Bi	5.7	Werner et al. ⁵⁰
Cu	3.4	Babar & Weaver ⁵¹
Ga	8.5	McMahon et al. ⁴³
Mg	6.4	Hagemann et al. ⁵²
Sn	10.6	Palik ⁵³

expression is close to zero. This condition gives rise to a pronounced oscillation of free electrons, a substantial enhancement of the electric field in proximity to the nanoparticle, and elevated levels of light absorption and scattering at a particular resonant frequency. This resonant frequency corresponds to a value at which the real part of the nanoparticle’s permittivity approximates -2 times the real part of the surrounding medium’s permittivity. In the context of a metallic nanoparticle with dielectric function ϵ in air, the Fröhlich condition is $\Re[\epsilon(E_F)] = -2$. The value of E_F then indicates the theoretical energy of the LSPRs in a small nanosphere in the air. The energy of LSPRs can be further tuned by the dielectric environment that embeds the nanostructure and by enlargement of the nanostructure and its morphology. Table 1 summarizes the Fröhlich energy E_F for selected non-noble metals.

Aluminium

Aluminium is the 12th most abundant element in the universe. It is a soft, nonmagnetic, ductile, and low density metal with a melting temperature of 660.3°C. It is a CMOS compatible material. It has a great affinity for oxygen and a protective oxide layer (Al_2O_3) on the surface that forms rapidly when exposed to air, stabilizing at 2.5–3 nm thickness in hours and acts as a self-limiting passivation layer preventing further oxidation for at least 30 days.⁵⁷ Its biocompatibility is generally good. However, for direct contact with the body, surface treatments, such as anodizing, are crucial to enhance corrosion resistance and prevent adverse reactions by creating a protective oxide layer. Aluminium has emerged as a promising plasmonic material characterized by a high bulk plasma frequency of approximately 15 eV,

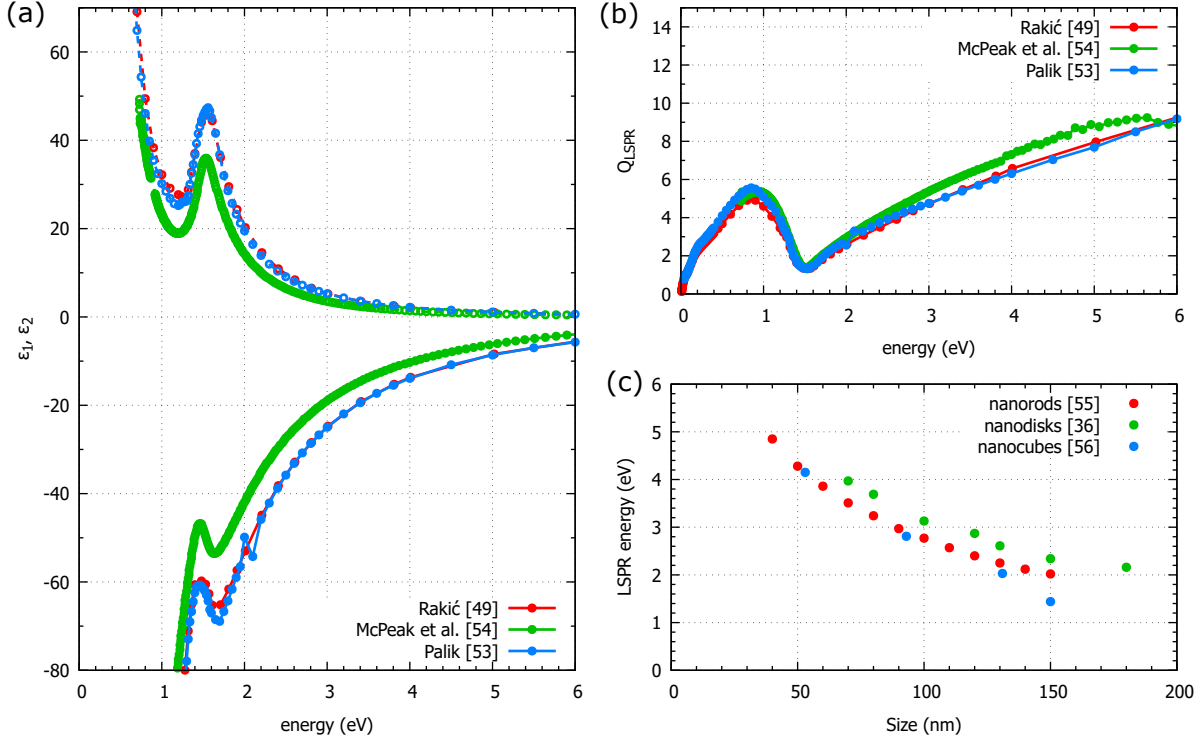


Figure 2: Aluminium plasmonics: (a) Experimental dielectric functions of aluminium by Rakić,⁴⁹ McPeak et al.,⁵⁴ and Palik.⁵³ The real part (ϵ_1) is plotted by filled circles connected with a solid line and the imaginary part (ϵ_2) by empty circles connected with a dashed line. (b) Theoretical quality factors of LSPRs derived from these dielectric functions as $Q_{\text{LSPR}} = -\epsilon_1/\epsilon_2$. (c) LSPR energy as a function of size of aluminium nanostructures, namely longitudinal dipole mode in aluminium nanorods,⁵⁵ in-plane dipole mode in aluminium nanodisks,³⁶ and dipole mode in aluminium nanocubes.⁵⁶

resulting from the high electron density with 3 conduction electrons per atom. The negative real part of the dielectric function extends well into the ultraviolet range, allowing LSPR to reach the deep ultraviolet through visible to near-infrared regions of the spectrum. However, it has a spectrally localized narrow-band interband transition around 1.5 eV that may lead to a strong interaction with LSPR resulting in hybridization.⁵⁸

Figure 2a shows a comparison of three experimental dielectric functions of aluminium available in the literature, namely by Rakić,⁴⁹ McPeak et al.,⁵⁴ and Palik.⁵³ There are no significant differences. The peak in the imaginary part of the dielectric function around 1.5 eV corresponds to the narrow-band interband transition. The real part of the dielectric function reaches highly negative values, promising a good plasmonic activity over the entire energy

range from the ultraviolet to the infrared spectral region. Figure 2b shows the theoretical quality factors of the LSPRs derived from these dielectric functions as $Q_{\text{LSPR}} = -\epsilon_1/\epsilon_2$. There are no significant differences between the theoretical quality factors derived from the three examples of dielectric functions. It reaches values between 2 and 6 in the near-infrared, 2 to 6 in the visible, and 6 to 10 in the ultraviolet spectral region. The lowest value of 2 in the red part of the spectrum is attributed to the narrow-band interband transition around 1.5 eV.

Aluminium nanostructures can be manufactured using various lithography techniques, such as electron beam lithography, nanosphere lithography, nanoimprint lithography, and photolithography, or by chemical synthesis of nanoparticles in various geometries.^{56,59,60} LSPR in various types of aluminium nanostructures have been studied, such as nanorods,^{55,60} nanodisks,³⁶ nanodisk arrays,⁶¹ and nanocubes,⁵⁶ demonstrating their wide tunability from ultraviolet through the visible to near-infrared spectral region. The influence of the oxide layer on the LSPR in aluminium nanostructures was studied, resulting in a redshift in the resonant frequency and a decrease in the scattering efficiency with an increasing oxide fraction.^{36,62} aluminium nanostructures can degrade by photocorrosion under strong ultraviolet light exposure that may be prevented by depositing a protective layer 5 nm TiO_2 or a protective layer 10 nm SiO_2 .⁶³

Figure 2c shows the dipole LSPR energy as a function of the size of aluminium nanostructures for three representative systems available in the literature, namely the longitudinal dipole mode in nanorods,⁵⁵ the in-plane dipole mode in nanodisks,³⁶ and the dipole mode in nanocubes.⁵⁶ The results show a wide tunability of aluminium nanostructures from the ultraviolet region for the size of structures below 100 nm to the visible spectral region for the size of structures up to 200 nm. The structures above 200 nm are intended to represent the plasmonic platform for the near-infrared spectral region.

There are numerous applications for the plasmonic properties of aluminium nanostructures, including surface-enhanced Raman spectroscopy,⁶⁴ plasmon-enhanced fluorescence,^{65,66}

surface-enhanced infrared absorption,⁶⁷ and biosensing.⁶⁸ In addition, a wide field of applications for such nanoparticles in photocatalysis was introduced, including water oxidation,⁶⁹ methylene blue decomposition,⁷⁰ hydrogen dissociation,⁷¹ and the reverse Boudouard reaction, which is an endothermic heterogeneous process occurring at high temperatures where carbon dioxide reacts with solid carbon to produce high-purity carbon monoxide.⁷² Consequently, aluminium is a well established plasmonic material with deep-explored plasmonic properties that is used in a wide range of applications.

Bismuth

Bulk bismuth is a metal with a melting temperature of 271.5 °C. It is generally considered biocompatible. The only known bodily harm caused by bismuth is inflammation of the lungs after inhalation of fine bismuth powder, which is caused by mechanical irritation of the tissue. However, when bismuth is introduced into the body in other forms, no negative effects on mammals have been observed, even at doses as high as 1000 mg per 1 kg of body mass.^{75,76} Bismuth in the form of thin polycrystalline layers appears to be chemically stable and resistant to oxidation under ambient conditions; however, bismuth can easily be oxidized in an oxygen-reactive atmosphere, such as oxygen plasma, or by annealing under an oxygen atmosphere.⁷⁴ As a result, bismuth can be easily covered by a few nanometers of oxide layer that may act as an insulator and, for example, prevent charge transfer in catalytic reactions. The low effective mass of free electrons and the dielectric function of bismuth suggest that it is an attractive plasmonic material suitable for plasmonics spanning from the near-infrared to the ultraviolet spectral region.^{43,77,78} Furthermore, the extraordinary properties of bismuth, including quantum confinement,⁷⁹ temperature-induced metal-to-semiconductor transition,^{80,81} and high values of the Seebeck coefficient,⁸² when combined with its plasmonic performance, have the potential to yield new applications. The biocompatibility, high atomic number, and accessible functionalization of bismuth nanoparticles make them

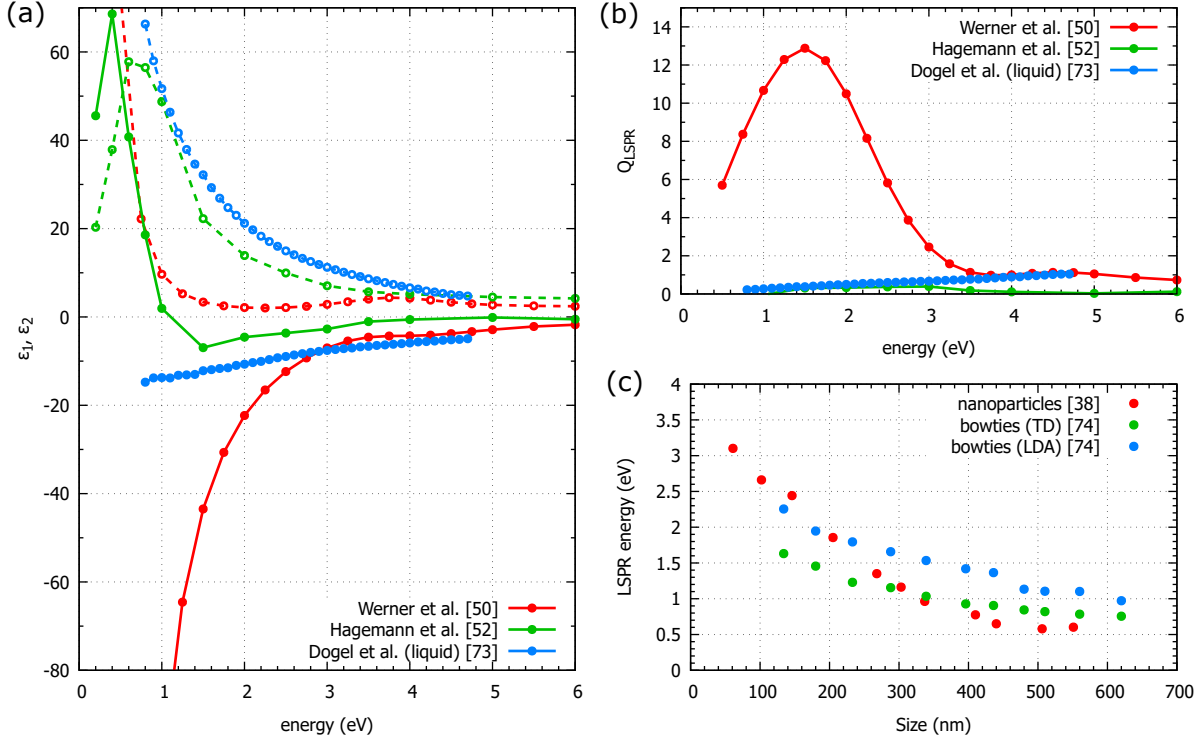


Figure 3: Bismuth plasmonics: (a) Experimental dielectric functions of bismuth by Werner et al.,⁵⁰ Hagemann et al.,⁵² and for the liquid bismuth by Dogel et al.⁷³ The real part (ϵ_1) is plotted by filled circles connected with a solid line and the imaginary part (ϵ_2) by empty circles connected with a dashed line. (b) Theoretical quality factors of LSPRs derived from these dielectric functions as $Q_{\text{LSPR}} = -\epsilon_1/\epsilon_2$. (c) LSPR energy as a function of size of bismuth nanostructures, namely dipole mode in bismuth nanoparticles on silicon dioxide membrane,³⁸ transverse dipole (TD) and longitudinal antibonding dipole (LDA) mode in bowties on silicon nitride membrane manufactured by focused ion beam lithography.⁷⁴

a compelling candidate as a contrast enhancing agent in medical X-ray imaging and computational tomography techniques.^{83,84} Furthermore, their recently reported photocatalytic and photothermal properties also make them attractive for use in photothermal cancer therapies,^{76,85} environmental remediation,^{86–88} and energy storage.⁸⁹

Figure 3a shows a comparison of three experimental dielectric functions of bismuth available in the literature, namely by Werner et al.,⁵⁰ Hagemann et al.,⁵² and for the liquid bismuth by Dogel et al.⁷³ There are significant differences in these dielectric functions. The dielectric function of Werner et al.⁵⁰ indicates that bismuth is a suitable plasmonic material, whereas the other two indicate that it is not. Figure 3b shows the theoretical quality

factors of the LSPRs derived from these dielectric functions. Taking the dielectric function of Werner et al.,⁵⁰ bismuth represents a good plasmonic platform for the near-infrared and visible spectral region with the theoretical quality factor of the LSPRs reaching values from 2 to 13. In contrast, the use of the other two dielectric functions results in the theoretical quality factor of the LSPRs below 1. Therefore, it is necessary to select a suitable dielectric function for this material when considering its plasmonic applications.

The potential combination of plasmonic applications and the extraordinary properties of bismuth has driven research on circular or spherical bismuth nanostructures,^{37,38,90–93} bismuth nanowires,^{94,95} and nanostructured bismuth thin films.^{37,74,91,93,96} Most studies on the plasmonic response of chemically synthesized bismuth nanoparticles have been limited only to investigations of plasmonic performance using far-field optical spectroscopy. The main constraint of this method is that it mostly measures the overall response of an ensemble of nanoparticles in a large volume of solution containing nanoparticles of various sizes resulting in a difficult isolation of a single nanoparticle contribution. The exploration of the spectral tunability of LSPRs in individual bismuth nanostructures as a function of their size has recently been investigated by electron energy loss spectroscopy for monocrystalline spherical bismuth nanoparticles,³⁸ as well as bismuth plasmonic antennas manufactured by focused ion beam lithography,⁷⁴ and the theoretically predicted spectral interval that extends from the near-infrared to the ultraviolet was confirmed for LSPRs in bismuth nanostructures.

Figure 3c shows the dipole LSPR energy as a function of the size of bismuth nanostructures for two representative systems available in the literature, namely the dipole mode in bismuth nanoparticles on the silicon dioxide membrane,³⁸ and the transverse dipole (TD) and longitudinal antibonding dipole (LDA) mode in bowties on the silicon nitride membrane manufactured by focused ion beam lithography.⁷⁴ The results show a wide tunability of bismuth nanostructures from the ultraviolet region for the size of structures below 50 nm through the visible spectral region for the size of structures up to 200–300 nm depending on the shape to the near-infrared spectral region for larger structures.

In addition, bismuth has been considered as a viable substitute for gold. A direct comparison of the LSPR energies in bismuth and gold bowties suggests that bismuth can be considered as an alternative material to gold.⁷⁴ The Q factors of the bismuth antennas are marginally lower than those of gold; however, this disadvantage is counterbalanced by their consistent performance even at higher plasmon energies. Further research in bismuth-based plasmonics could include thin-film optimization to enhance the properties of bismuth antennas. In addition, a deeper understanding of the metal-to-semiconductor transition in very thin bismuth layers has the potential to be applicable in the low-temperature active plasmonic devices. In the case of nanoparticles, the main open question is their possible functionalization, which is crucial for any application in biochemistry.

Copper

Copper is a soft, malleable, and ductile metal with very high thermal and electrical conductivity. Its melting temperature is 1084.6 °C. It is a CMOS compatible material. Copper is an indispensable trace metal element in the human body, as it being an important component and catalytic agent of many enzymes and proteins, while copper-based materials generally exhibit antibacterial effects and good biocompatibility.⁹⁹ Copper does not react inherently with water; however, it slowly reacts with atmospheric oxygen, resulting in the formation of a layer of brown-black copper oxide. This layer functions as a protective barrier that protects the underlying metal from further corrosion. A green layer of copper carbonate is often visible on aged copper structures. Copper tarnishes when exposed to sulfur compounds, with which it reacts to form various copper sulfides. Fortunately, copper nanostructures can be protected from harsh environments by protective coatings, such as thin oxide films, including alumina (Al_2O_3), hafnia (HfO_2), or titania (TiO_2), deposited by atomic layer deposition onto substrate-based copper nanostructures. The resulting nanostructures are resistant to oxidation, high temperatures, and aqueous, acidic, and alkaline solutions without unduly

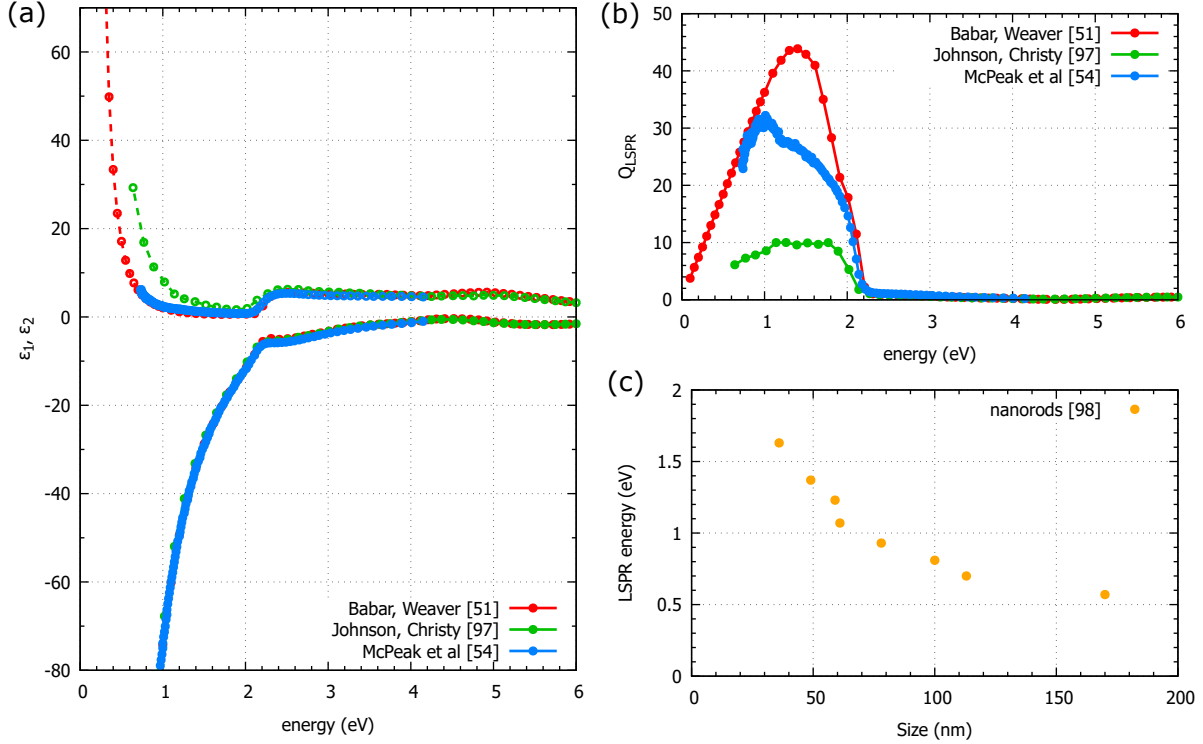


Figure 4: Copper plasmonics: (a) Experimental dielectric functions of copper by Babar and Weaver,⁵¹ Johnson and Christy,⁹⁷ and McPeak et al.⁵⁴ The real part (ϵ_1) is plotted by filled circles connected with a solid line and the imaginary part (ϵ_2) by empty circles connected with a dashed line. (b) Theoretical quality factors of LSPRs derived from these dielectric functions as $Q_{\text{LSPR}} = -\epsilon_1/\epsilon_2$. (c) LSPR energy as a function of size of copper nanoparticles, namely longitudinal dipole mode in copper nanorods dispersed in tetrachloroethylene.⁹⁸

influencing important plasmonic properties.¹⁰⁰

Figure 4a shows a comparison of three experimental dielectric functions of bismuth available in the literature, namely by Babar and Weaver,⁵¹ Johnson and Christy,⁹⁷ and McPeak et al.⁵⁴ There seem to be no significant differences. The real part of the dielectric function reaches highly negative values in the infrared and visible spectral range, promising good plasmonic activity, especially in the infrared spectral region. The imaginary part of the dielectric function increases around 2.1 eV due to the interband transition. Figure 4b shows the theoretical quality factors of the LSPRs derived from these dielectric functions. Taking the dielectric function of Babar and Weaver,⁵¹ copper represents a perfect plasmonic platform for the near-infrared and red visible spectral region (below 2 eV) with an excellent

theoretical quality factor of LSPRs that reach values of 20 to 45. The use of the other two dielectric functions results in lower quality factors, but still reaching very high values of 10 to 30 in the near-infrared spectral region. Therefore, copper is supposed to be an excellent plasmonic platform for the near-infrared and visible spectral region.

Copper nanoparticles of various shapes can be synthesized using multiple strategies, including polyol synthesis with effective control over their morphology,¹⁰¹ disproportionation reaction in oleylamine solvent, providing shape-selective synthesis of spherical and cubic nanocrystals with a very narrow size distribution,¹⁰² as well as colloidal synthesis¹⁰³ or plasmon-driven synthesis.¹⁰⁴ Although localized surface plasmons in copper are strongly damped by the interband transition above 2.1 eV,¹⁰⁵ they are comparable to gold in a low loss window extending from 1.6 to 2.0 eV.¹⁰⁶ Finally, elongated copper nanostructures sustain spectrally sharp visible to infrared plasmons of a quality factor similar to that of their silver counterparts; therefore, copper is emerging as an attractive, cheap and abundant material platform for high-quality plasmonics in elongated nanostructures.¹⁰⁷ The longitudinal dipole mode of localized surface plasmons in copper nanorods was proved to be tunable from 0.6 to 1.6 eV by their aspect ratio.⁹⁸

Figure 4c shows the longitudinal dipole mode of LSPRs in copper nanorods⁹⁸ that cover mostly the near-infrared spectral region with nanostructure size between 30 and 300 nm. The larger structures are intended to represent the plasmonic platform for the infrared spectral region. Consequently, copper is supposed to be a promising plasmonic material in the red part of the visible and infrared spectral regions.

Nanostructured copper has been demonstrated to allow the conversion of carbon dioxide (CO_2) into a variety of reducing products by electrocatalysis.¹⁰⁸ Copper nanoparticles with intense visible region surface plasmon absorption bands were found to be excellent nonlinear scatterers.¹⁰⁹ Their applications include refractive index sensing, surface-enhanced Raman spectroscopy, single nanoparticle spectroscopy, or selective catalysis.¹¹⁰ Surface-enhanced Raman spectroscopy of rhodamine B and photocatalysis in the paranitrophenol reduc-

tion reaction was demonstrated for hexagonal and cubic copper nanostructures.¹⁰¹ Copper nanoparticles were found to be an affordable plasmonic heater for photothermal applications including solar-vapor generation and driving temperature-dependent color changes in thermochromic molecules.¹¹¹ They were used in an interfacial solar steam generation system that performs solar desalination of water.¹¹² Furthermore, they improve the performance of organic photovoltaics.¹¹³ In addition, the plasmonic properties of copper oxides (Cu_2O and Cu_3O_2)¹¹⁴ and copper monosulfide (CuS)¹¹⁵ have been discussed. Further research in copper-based plasmonics could include thin-film optimization to explore and optimize the properties of copper antennas fabricated by lithography.

Gallium

Bulk gallium is a metal with a melting temperature of 29.7°C . It is a non-toxic material that is acceptable to the environment.^{116,117} In addition, gallium has several solid-state phases, namely α -gallium, β -gallium, γ -gallium, δ -gallium, ϵ -gallium, gallium-II and gallium-III, which allow for a variety of phase-changing systems.³¹ The dielectric properties of gallium are well explored by theoretical models, but there are not many measured dielectric functions. The liquid phase, γ phase, and δ phase of gallium has a nearly Drude-like optical response from the infrared to ultraviolet spectral region, while the α and β phases exhibit interband absorption in the red and green.^{30,31,118,119} Fortunately, this absorption is not strong enough to completely suppress plasmonic resonances.³⁰ Finally, gallium offers facile and scalable preparation and good stability for nanoparticles.

Figure 5a shows a comparison of the experimental dielectric functions of gallium available in the literature, namely the dielectric functions of liquid gallium by Knight et al.³⁹ and Dogel et al.,⁷³ and solid gallium by Knight et al.³⁹ and McMahon et al.⁴³ There are no significant differences in the two dielectric functions for the same phase. The major differences arise from the liquid to solid phase change. In the case of liquid gallium, the real part of the

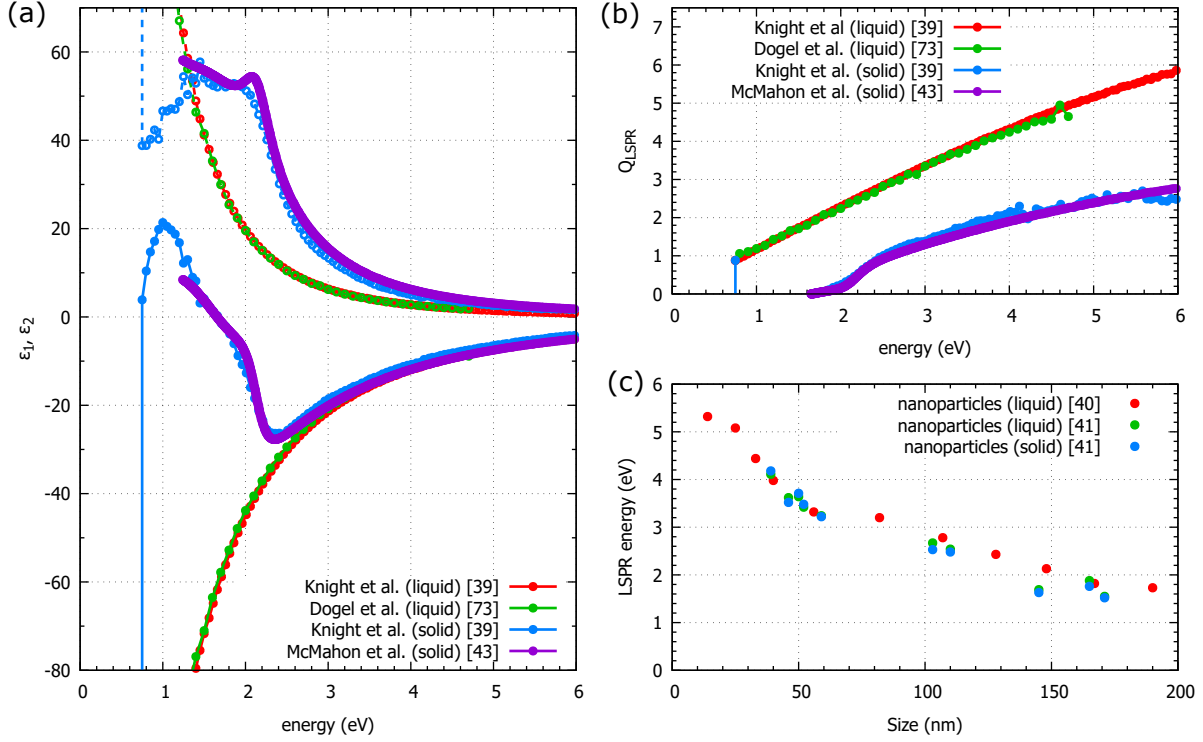


Figure 5: Gallium plasmonics: (a) Experimental dielectric functions of liquid gallium by Knight et al.³⁹ and Dogel et al.,⁷³ and solid gallium by Knight et al.³⁹ and McMahon et al.⁴³ The real part (ϵ_1) is plotted by filled circles connected with a solid line and the imaginary part (ϵ_2) by empty circles connected with a dashed line. (b) Theoretical quality factors of LSPRs derived from these dielectric functions as $Q_{LSPR} = -\epsilon_1/\epsilon_2$. (c) LSPR energy as a function of size of gallium nanoparticles, namely in-plane dipole mode in liquid⁴⁰ and liquid and solid⁴¹ gallium nanoparticles on a silicon nitride membrane.

dielectric function reaches highly negative values, promising a good plasmonic activity over the entire energy range from the ultraviolet to the infrared spectral region. In the case of solid gallium, the real part of the dielectric function increases below 2 eV, promising good plasmonic activity in the ultraviolet and visible spectral region. Figure 5b shows the theoretical quality factors of the LSPRs derived from these dielectric functions. In the case of liquid gallium, it increases with the energy starting around 1 at 1 eV and reaching the value of 6 at 6 eV. In the case of solid gallium, it increases with the energy starting around 1 at 2.5 eV and reaching a value of 2.5 at 6 eV. Consequently, gallium is supposed to be a suitable plasmonic platform, especially for the ultraviolet spectral region.

Gallium nanoparticles can be prepared using various bottom-up fabrication techniques

such as colloidal synthesis,^{120,121} optically regulated self-assembly,¹²² molecular beam epitaxy,¹²³ atomic beam evaporation,¹²⁴ and Joule-effect thermal evaporation.¹²⁵ Importantly, the low melting temperature of gallium allows low-temperature fabrication with low energy consumption. Despite the fact that the phase diagram of gallium nanoparticles was introduced,³¹ there are several discrepancies that need to be taken into account, as it contradicts several experimental works. First, at room temperature (25 °C) gallium nanoparticles are in the form of a supercooled liquid.^{40,41,120,126} Second, nanoparticles with diameters ranging from 50 to 300 nm were found to crystallize to the β phase of gallium with a freezing temperature around -135 °C and a melting temperature around -20 °C.^{41,126} Third, nanoparticles smaller than 50 nm were found to crystallize in the δ phase of gallium.¹²⁰ Consequently, the phase diagram for gallium nanoparticles needs to be carefully updated and reformulated with respect to the experimental results. The size of the nanoparticles needs to be reflected, as well as possible effects of the substrate and the deposition method. Finally, another challenge could be the preparation of non-spherical shapes of nanoparticles, for example, by lithography or nanomolding.

The plasmonic properties of gallium nanoparticles have been well explored, showing a wide spectral tunability from the ultraviolet to the near-infrared spectral region at room temperature.^{39,40,127} Furthermore, the impact of the liquid to solid phase transition on the plasmonic properties of gallium nanoparticles has been explored, while differences in the LSPR energies between liquid gallium and β -gallium nanoparticles are minor.⁴¹ As a result, the energy shift related to the temperature-induced phase change is relatively small to be utilized, for example, as a temperature sensor. The performance of gallium nanoparticles is, in the case of temperature-dependent experiments, unaffected by the liquid to solid phase change of gallium, which is valuable for cryogenic temperature-suppressed non-radiative recombination in surface-enhanced Raman spectroscopy.^{128,129} In addition, plasmonic properties of Ga-Ga₂O₃ core-shell structures^{130,131} and gallium-indium¹³² and gallium-silver¹³³ alloys have been reported.

Figure 5c shows the dipole LSPR energy as a function of the size of gallium nanoparticles available in the literature, namely the in-plane dipole mode in liquid⁴⁰ and liquid and solid⁴¹ lens-shaped gallium nanoparticles on a silicon nitride membrane. The results show a wide tunability of gallium nanostructures from the ultraviolet region for the size of structures below 50 nm to the visible spectral region for the size of structures up to 200 nm. In addition, the liquid gallium nanostructures above 200 nm are intended to represent the plasmonic platform for the near-infrared spectral region.

There are numerous applications for such nanoparticles, including DNA biosensing platforms,¹³⁴ luminescence enhancement of MoS₂ monolayers,¹³⁵ and surface-enhanced Raman spectroscopy applications.¹³⁶⁻¹³⁹ Further research in gallium-based plasmonics could include applications that utilize the room- to cryo-temperature stability of LSPR in gallium nanoparticles, Ga-GaN core-shell structures, or other alloys such as gallium-aluminium.

Magnesium

Magnesium is the sixth most abundant element on Earth. Bulk magnesium is a metal with a melting temperature of 650 °C. Magnesium is also a very important biogenic element. It is found in all green plants, where it is a component of chlorophyll. It is also one of the important biogenic elements in animal organisms. It is highly reactive and elemental magnesium is a strong reducing agent. It has a higher plasmonic quality factor than aluminium across the visible spectral region, making it an attractive framework for plasmonics. The hexagonal, folded, and kite-shaped shapes were theoretically expected from a modified Wulff construction for single crystal and twinned magnesium nanostructures, and their plasmonic properties have been introduced, highlighting the ability of magnesium to sustain LSPRs in the ultraviolet, visible, and near-infrared spectral region.¹⁴⁴

Figure 6a shows a comparison of three experimental dielectric functions of magnesium available in the literature, namely by Palm et al.,¹⁴⁰ Appusamy et al.,¹⁴¹ and Hagemann

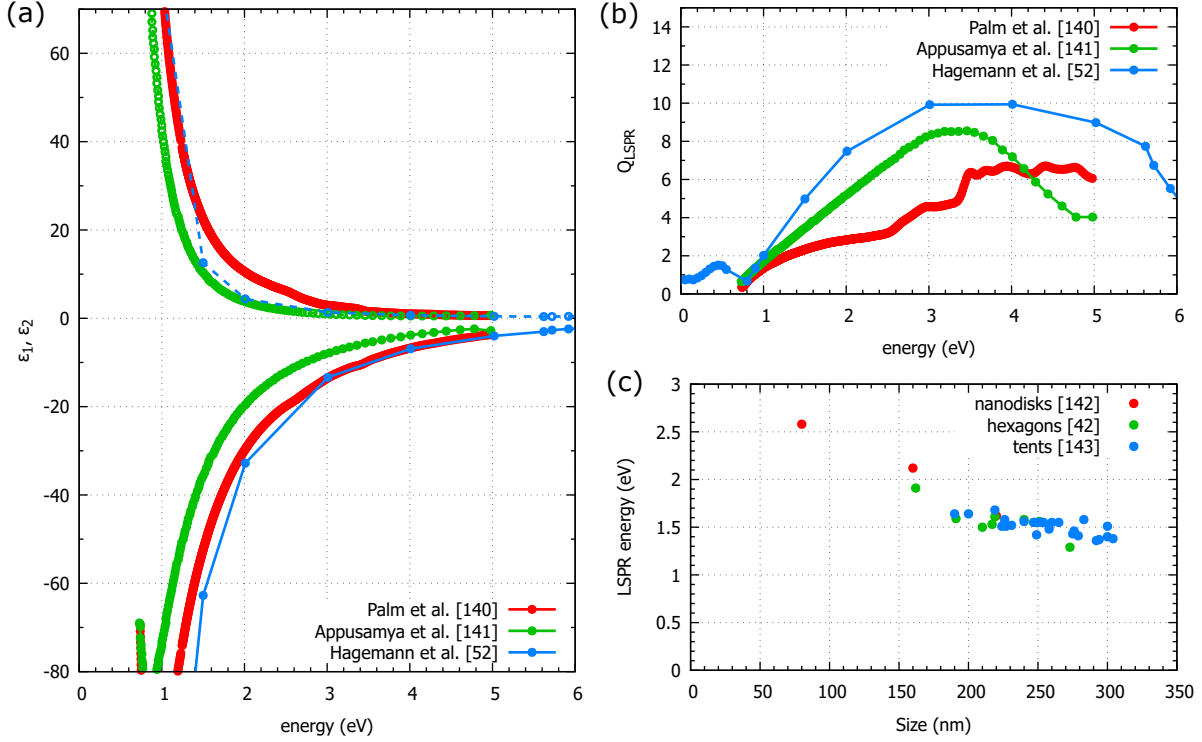


Figure 6: Magnesium plasmonics: (a) Experimental dielectric functions of magnesium by Palm et al.,¹⁴⁰ Appusamya et al.,¹⁴¹ and Hagemann et al.⁵² The real part (ϵ_1) is plotted by filled circles connected with a solid line and the imaginary part (ϵ_2) by empty circles connected with a dashed line. (b) Theoretical quality factors of LSPRs derived from these dielectric functions as $Q_{\text{LSPR}} = -\epsilon_1/\epsilon_2$. (c) LSPR energy as a function of size of magnesium nanostructures, namely magnesium nanodisks,¹⁴² hexagons,⁴² and tent-shaped structures.¹⁴³

et al.⁵² There seem to be no significant differences. However, they may still influence the simulation results, so the dielectric function should be chosen carefully. The real part of the dielectric function reaches highly negative values in the infrared and visible spectral range, promising good plasmonic activity. Figure 6b shows the theoretical quality factors of the LSPRs derived from these dielectric functions. They reach values between 3 and 10 in the visible and ultraviolet spectral regions. Consequently, magnesium is a suitable plasmonic platform in the ultraviolet and visible spectral region.

Magnesium nanostructures can be chemically synthesized^{42,143} as well as manufactured by colloidal hole-mask lithography¹⁴² or nanosphere lithography.¹⁴⁵ The stability of plasmonic magnesium nanoparticles can be improved by encapsulation in a polydopamine shell.¹⁴⁶

Full modal analysis of LSPR magnesium hexagons⁴² and tent-shaped structures¹⁴³ was performed.

Figure 6c shows the dipole LSPR energy as a function of the size of magnesium nanoparticles available in the literature, namely magnesium nanodisks,¹⁴² hexagons,⁴² and tent-shaped structures.¹⁴³ The results show a relatively narrow tunability of magnesium nanostructures from the visible region for the size of structures between 50 and 200 nm to the near-infrared spectral region for the larger structures. In addition, smaller magnesium nanostructures are intended to represent the plasmonic platform for the ultraviolet spectral region.

The potential of magnesium based nanostructures for surface-enhanced Raman spectroscopy is demonstrated with enhancement factors of around 100 for pure magnesium and around 1000 for magnesium with palladium.¹⁴⁷ Magnesium is more efficient at converting light into heat than gold at near-infrared wavelengths, so magnesium nanoparticles can be used as inexpensive and biodegradable photothermal platforms.¹⁴⁸ In addition, magnesium nanoparticles have been introduced in biomedical applications as a platform for hydrogen cancer therapy.¹⁴⁹ Magnesium nanohelices were studied as chiral nanoparticles having a remarkable chiroptical effect in the ultraviolet region together with an enhanced LSPR sensitivity.¹⁵⁰ A magnesium plasmonic device whose transmittance can be tuned by water can serve as an optical sensor to measure ambient humidity and monitor changes in humidity over time.¹⁵¹ Finally, palladium-magnesium bimetallic nanocomposites were shown to be promising highly selective hydrogenation catalysts under conventional thermally-driven conditions.¹⁵²

Moreover, magnesium nanostructures can be used as a platform for dynamic plasmonics. It is based on a reversible phase transition between the metallic state of pure magnesium (Mg) and the dielectric state of magnesium hydride (MgH₂) through hydrogenation and dehydrogenation under hydrogen (H₂) and oxygen (O₂) atmosphere, respectively.^{142,153} Alternatively, this phase transition may be driven by hydrogenation in the hydrogen atmosphere and dehydrogenation by thermal desorption of hydrogen in the argon atmosphere at 95 °C.¹⁵⁴

Tin

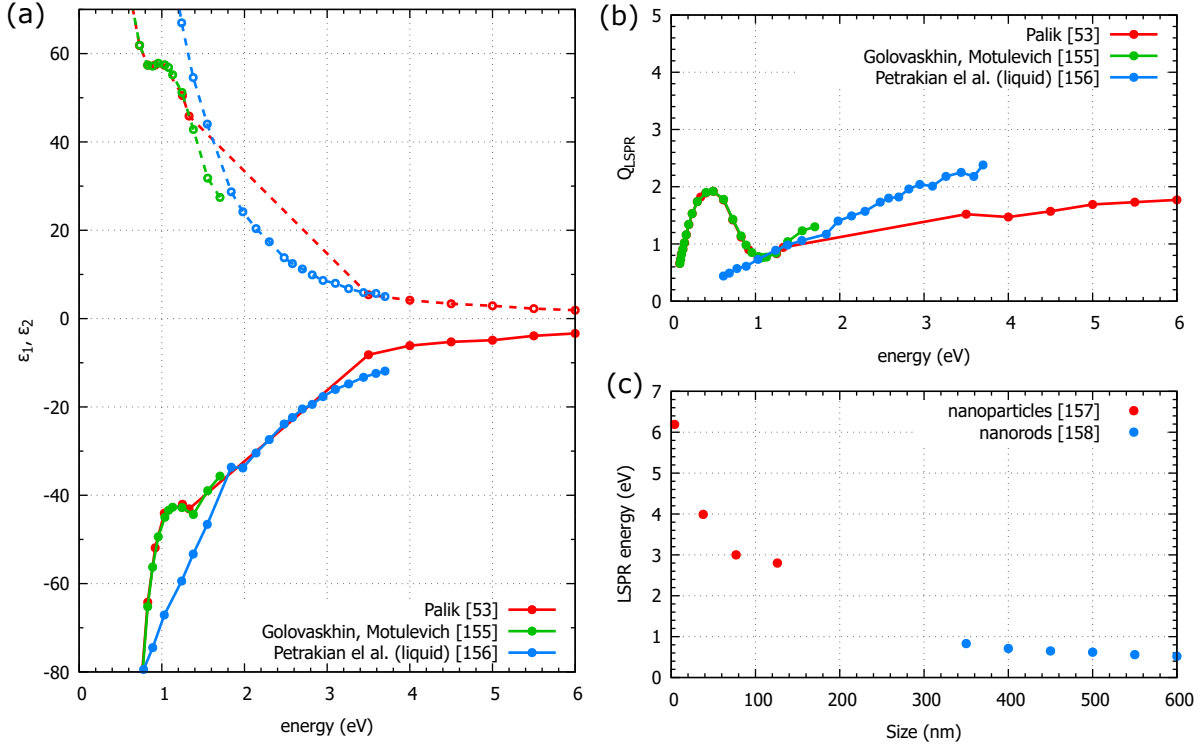


Figure 7: Tin plasmonics: (a) Experimental dielectric functions of tin by Palik,⁵³ Golovashkin and Motulevich,¹⁵⁵ and for the liquid tin by Petrakian et al.¹⁵⁶ The real part (ϵ_1) is plotted by filled circles connected with a solid line and the imaginary part (ϵ_2) by empty circles connected with a dashed line. (b) Theoretical quality factors of LSPRs derived from these dielectric functions as $Q_{\text{LSPR}} = -\epsilon_1/\epsilon_2$. (c) LSPR energy as a function of size of tin nanostructures, namely tin spherical nanoparticles¹⁵⁷ and tin nanorods on glass.¹⁵⁸

Tin is a soft, malleable, and ductile metal. The melting temperature of the bulk tin is 232 °C. However, the melting point is reduced to 150 °C for nanoparticles below 10 nm.^{159,160} The surface melting of a single tin nanoparticle with a diameter of 47 nm was observed at 200–225 °C by in situ transmission electron microscopy showing a wide hysteresis, as the crystallization of the liquid tin nanoparticle occurred with a large overcooling at 100 °C.¹⁶¹ The wide hysteresis (around 130 °C) of the solid-liquid phase change of the tin nanoparticles was determined by optical excitation measurements of the localized surface plasmon resonance in the tin nanoparticles.¹⁶² Moreover, the local thermal expansion coefficient of single liquid tin nanoparticles was evaluated.¹⁶³ In addition, tin has several solid-state phases. β -tin

(also called white tin) is the allotrope of tin that is stable at and above room temperature. It is metallic with a body-centered tetragonal crystal structure. In cold β -tin tends to spontaneously transform into α -tin, which is a phenomenon known as the tin pest. α -tin (or gray tin) is a nonmetallic form with a diamond cubic crystal structure that is stable below 13 °C. At temperatures above 160 °C and pressures above several gigapascals γ -tin and σ -tin are reported.¹⁶⁴

Figure 7a shows a comparison of three experimental dielectric functions of tin available in the literature, namely by Palik,⁵³ Golovashkin and Motulevich,¹⁵⁵ and for the liquid tin by Petrakian et al.¹⁵⁶ There seem to be no significant differences. However, all of these dielectric functions suffer from their narrow spectral range and low number of data points. The real part of the dielectric function reaches highly negative values, promising plasmonic activity over the entire energy range from the ultraviolet to the infrared spectral region. Figure 7b shows the theoretical quality factors of the LSPRs derived from these dielectric functions. They reach values between 1 and 2, predicting that tin is not a perfect plasmonic material. However, further experiments are required to obtain a more accurate dielectric function of tin.

Tin nanostructures can be synthesized chemically,¹⁵⁷ as well as manufactured by electron beam lithography¹⁶⁵ or sequential self-assembly (chemical dealloying).^{166,167} The plasmonic properties of tin nanoparticles have been thoroughly explored, including a size-dependent evolution of plasmonic modes and surface-enhanced Raman spectroscopy performance of β -tin nanoparticles¹⁵⁷ and tuning the plasmon resonance of metallic tin nanocrystals dispersed in silicon dioxide and amorphous silicon matrix.¹⁶⁸ Moreover, the optical transmission of hexagonal oriented tin nanobars was discussed to create a plasmonic meatusurface for the near-infrared spectral region.¹⁵⁸ Tin disks with a diameter of 155 nm and height of 50 nm reveal a transmission peak around 2.3 eV and their sensing possibilities have been discussed.¹⁶⁵

Figure 7c shows the dipole LSPR energy as a function of the size of tin nanoparticles available in the literature, namely tin spherical nanoparticles¹⁵⁷ and tin nanorods on glass.¹⁵⁸

The results show a wide tunability of the tin nanostructures from the ultraviolet region for the size of structures below 100 nm to the near-infrared spectral region for structures of length between 300 and 600 nm. In addition, tin nanostructures with a size between 100 and 250 nm are intended to represent the plasmonic platform for the visible spectral region.

The coupling of localized surface plasmons was explored in tin nanoparticles dispersed in a copper matrix.¹⁶⁶ The Janus nanoparticle was effectively formed by introducing a silver nanoantenna active in the visible light spectral region on one side of a tin nanoparticle with localized surface plasmons located in the ultraviolet range.¹⁶⁷ In addition, the Begrenzung effect that leads to the suppression of surface plasmons was discussed for tin nanoparticles encapsulated in silicon nitride.¹⁶⁹ Tin nanoparticles have been proposed as a relevant additive to the photoactive silicon layer in plasmon assisted silicon solar cells, as tin is in the same group IV as silicon and therefore does not introduce any additional energy level into the band gap nor create recombination centers.¹⁷⁰

Other non-noble metals

The following non-noble metals, antimony (Sb), chromium (Cr), indium (In), lead (Pb), molybdenum (Mo), nickel (Ni), potassium (K), selenium (Se), sodium (Na), tellurium (Te), titanium (Ti), tungsten (W), and zinc (Zn), are less frequently used in plasmonic applications. Therefore, we will discuss them briefly below. The rationale underlying this concise synopsis is chiefly the circumscribed extent of general understanding. Finally, we note that the list does not contain all non-noble metals, so there is still a possibility to pioneer the plasmonic properties of some of the unexplored non-noble metals.

Antimony

The first non-noble metal in this section is antimony. Tunable localized surface plasmon resonances have been reported in biocompatible antimony nanopolyhedrons with high pho-

tothermal conversion efficiency and good photothermal stability.¹⁷¹

Chromium

The weak plasmonic activity of chromium was theoretically predicted,³⁵ but there are only a few applications in the literature that include chromium microrods¹⁷² and chromium nitride (Cr_2N) nanoparticles.¹⁷³

Indium

In the case of indium, the field of applications is slightly larger. Indium nanoparticles were found to be a promising candidate for deep-ultraviolet plasmonics.¹⁷⁴⁻¹⁷⁶ Indium nanocrystals were also used for the selective enhancement of blue upconversion luminescence,¹⁷⁷ to improve the efficiency of silicon solar cells,¹⁷⁸ and for surface-enhanced Raman scattering.¹⁷⁹

Lead

The plasmonic properties of lead nanoparticles have not been explored in detail. However, the plasmonic response of lead films deposited on nanostructured substrates was investigated, showing that lead can be used as an alternative plasmonic material within the visible to near-infrared spectral range.¹⁸⁰

Molybdenum

Localized surface plasmon resonances were introduced for molybdenum microstructures.¹⁸¹ However, with respect to their size and spatial distribution, it is disputable whether the observed effect can be assigned to the localized surface plasmon resonance or not. As a result, there has been no systematic study of plasmon resonances in individual molybdenum nanostructures. In addition, tunable plasmonic resonance was observed in molybdenum oxides (MoO_3 and MoO_{3-x})^{182,183} and a strong surface plasmon resonance in molybdenum

nitride (MoN) nanosheets has been introduced as a promising surface enhanced Raman scattering platform¹⁸⁴

Nickel

In the case of nickel, its plasmonic properties, which have been thoroughly explored,¹⁸⁵ can be combined with its magnetic properties. In this sense, plasmon-induced demagnetization and magnetic switching in nickel nanoparticle arrays was introduced.¹⁸⁶

Potassium

Potassium plasmonic nanostructures were fabricated using a thermo-assisted nanoscale embossing technique to create nanostructures with varying periodicities that support high-quality surface plasmon modes.¹⁸⁷ In addition, sodium-potassium liquid alloys have been discussed.¹⁸⁷ However, there is no systematic study of localized surface plasmons in individual potassium nanostructures.

Selenium

The plasmonic activity has been reported for selenium nanoparticles that revealed a significant surface plasmon resonance peak at 4.7 eV, and their protective effect against chromium tubular necrosis has been discussed.¹⁸⁸

Sodium

Sodium is predicted to be an ideal plasmonic material with very low optical loss across visible to near-infrared. A scalable fabrication method for sodium nanostructures was developed by combining phase-shift photolithography and a thermo-assisted spin-coating process. Using this method, sodium nanopit arrays were manufactured with varying periodicity that revealed tunable surface plasmon polariton modes ranging from visible to near-infrared.¹⁸⁹ In

addition, hot electron dynamics has been investigated in nanostructured sodium thin films on polyurethane supports, showing a unique early time response that provides key information on sodium-based plasmonics.¹⁹⁰ However, there is no systematic study of localized surface plasmons in individual sodium nanostructures.

Tellurium

Tellurium is the first reported material that simultaneously has plasmonic-like and all-dielectric properties in the solar radiation region. Tellurium nanoparticles with a wide size distribution were demonstrated to absorb more than 85% solar radiation throughout the spectrum, so it can be expected to be an advanced photothermal conversion material for solar-enabled water evaporation.¹⁹¹

Titanium

The weak plasmonic activity of titanium was theoretically predicted,³⁵ but in the literature no applications have been reported for pure titanium nanostructures. However, titanium nitride (TiN) is considered an alternative ceramic platform for plasmonic applications.^{192,193}

Tungsten

Characteristics of localized surface plasmons of tungsten nanowires with different diameters and lengths have been explored,¹⁹⁴ but no direct application has been reported. However, tungsten oxides, namely WO_{3-x} with abundant oxygen vacancies^{195,196} and $\text{W}_{18}\text{O}_{49}$ modified with HCl,¹⁹⁷ have been used as nonmetallic plasmonic catalysts.

Zinc

It has been experimentally and numerically confirmed that silica-dispersed zinc nanoparticles exhibit two optical extinction peaks that were ascribed to surface plasmon resonances in the

broad sense.^{198–200} However, a comprehensive study of localized surface plasmon resonances is lacking. Furthermore, we note that zinc oxide (ZnO) nanoparticles represent a commonly used catalytic system^{201,202} that can be modified with noble metals to further enhance its properties.^{203,204}

Conclusions

In summary, this review of the literature dealing with the investigation of localized surface plasmons in non-noble metal nanoparticles provides an overview of the plasmonic properties of non-noble metals. We focused mostly on widely used non-noble plasmonic metals such as aluminium (Al), bismuth (Bi), copper (Cu), gallium (Ga), magnesium (Mg), and tin (Sn). In addition, the following less frequently used plasmonic non-noble metals are discussed, too: antimony (Sb), chromium (Cr), indium (In), lead (Pb), molybdenum (Mo), nickel (Ni), potassium (K), selenium (Se), sodium (Na), tellurium (Te), titanium (Ti), tungsten (W), and zinc (Zn). We compared the experimental dielectric functions and the theoretical quality factors of localized surface plasmon resonances calculated using them. In addition, we reviewed the spectral tunability of real nanostructures by plotting the dipole mode energy as a function of their size. Finally, examples of applications were briefly summarized for every metal.

Aluminium, bismuth, gallium, magnesium, and tin nanostructures offer wide tunability of the dipole mode with increasing their size from the ultraviolet region through the visible spectral region to the near-infrared spectral region. In addition, magnesium stands out as a chemically switchable plasmonic platform based on hydrogenation and dehydrogenation. Copper is supposed to be an excellent plasmonic platform for the near-infrared and red part of visible spectral region with an excellent theoretical quality factor of localized surface plasmon resonances reaching values of 20 to 45.

Our summary therefore compared the plasmonic properties of non-noble metals and

briefly introduced their potential to the readers. Nevertheless, the plasmonics of non-noble metals is still an open field with a huge potential for new discoveries. These may include a systematic study of less explored non-noble metals, introduction of any other non-noble metal to the plasmonic family, or development of new applications and fabrication protocols for large-scale devices.

Acknowledgement

This work is supported by the OP JAK Excellent Research program (project QM4ST, No. CZ.02.01.01/00/22_008/0004572), and Brno University of Technology (project No. FSI-S-23-8336). M.F. acknowledges the support of the Brno Ph.D. talent scholarship.

References

- (1) Maier, S. A. *Plasmonics: Fundamentals and Applications*; Springer US, 2007.
- (2) Mie, G. Beiträge zur Optik trüber Medien, speziell kolloidaler Metallösungen. *Annalen der Physik* **1908**, *330*, 377–445.
- (3) Novotny, L.; van Hulst, N. Antennas for light. *Nature Photonics* **2011**, *5*, 83–90.
- (4) Schuller, J. A.; Barnard, E. S.; Cai, W.; Jun, Y. C.; White, J. S.; Brongersma, M. L. Plasmonics for extreme light concentration and manipulation. *Nature Materials* **2010**, *9*, 193–204.
- (5) Kelly, K. L.; Coronado, E.; Zhao, L. L.; Schatz, G. C. The Optical Properties of Metal Nanoparticles: The Influence of Size, Shape, and Dielectric Environment. *The Journal of Physical Chemistry B* **2002**, *107*, 668–677.
- (6) Stockman, M. I.; Kneipp, K.; Bozhevolnyi, S. I.; Saha, S.; Dutta, A.; Ndukaife, J.;

- Kinsey, N.; Reddy, H.; Guler, U.; Shalaev, V. M. et al. Roadmap on plasmonics. *Journal of Optics* **2018**, *20*, 043001.
- (7) Knight, M. W.; Sobhani, H.; Nordlander, P.; Halas, N. J. Photodetection with Active Optical Antennas. *Science* **2011**, *332*, 702–704.
- (8) Smolyaninov, I. I.; Elliott, J.; Zayats, A. V.; Davis, C. C. Far-Field Optical Microscopy with a Nanometer-Scale Resolution Based on the In-Plane Image Magnification by Surface Plasmon Polaritons. *Physical Review Letters* **2005**, *94*, 057401.
- (9) Willets, K. A.; Van Duyne, R. P. Localized Surface Plasmon Resonance Spectroscopy and Sensing. *Annual Review of Physical Chemistry* **2007**, *58*, 267–297.
- (10) Boriskina, S. V.; Ghasemi, H.; Chen, G. Plasmonic materials for energy: From physics to applications. *Materials Today* **2013**, *16*, 375–386.
- (11) Baffou, G.; Quidant, R. Thermo-plasmonics: using metallic nanostructures as nano-sources of heat. *Laser & Photonics Reviews* **2012**, *7*, 171–187.
- (12) Szunerits, S.; Boukherroub, R. Sensing using localised surface plasmon resonance sensors. *Chemical Communications* **2012**, *48*, 8999.
- (13) Aćimović, S. S.; Ortega, M. A.; Sanz, V.; Berthelot, J.; Garcia-Cordero, J. L.; Renger, J.; Maerkl, S. J.; Kreuzer, M. P.; Quidant, R. LSPR Chip for Parallel, Rapid, and Sensitive Detection of Cancer Markers in Serum. *Nano Letters* **2014**, *14*, 2636–2641.
- (14) Zhang, X.; Li, X.; Reish, M. E.; Zhang, D.; Su, N. Q.; Gutiérrez, Y.; Moreno, F.; Yang, W.; Everitt, H. O.; Liu, J. Plasmon-Enhanced Catalysis: Distinguishing Thermal and Nonthermal Effects. *Nano Letters* **2018**, *18*, 1714–1723.
- (15) Zhang, Z.; Zhang, C.; Zheng, H.; Xu, H. Plasmon-Driven Catalysis on Molecules and Nanomaterials. *Accounts of Chemical Research* **2019**, *52*, 2506–2515.

- (16) Liu, S.; Wu, Z.; Zhu, Z.; Feng, K.; Zhou, Y.; Hu, X.; Huang, X.; Zhang, B.; Dong, X.; Ma, Y. et al. Quantifying the distinct role of plasmon enhancement mechanisms in prototypical antenna-reactor photocatalysts. *Nature Communications* **2025**, *16*, 2245.
- (17) Sheldon, M. T.; van de Groep, J.; Brown, A. M.; Polman, A.; Atwater, H. A. Plasmonic electric potentials in metal nanostructures. *Science* **2014**, *346*, 828–831.
- (18) Zheludev, N. I.; Prosvirnin, S. L.; Papasimakis, N.; Fedotov, V. A. Lasing spaser. *Nature Photonics* **2008**, *2*, 351–354.
- (19) Yu, N.; Genevet, P.; Kats, M. A.; Aieta, F.; Tetienne, J.-P.; Capasso, F.; Gaburro, Z. Light Propagation with Phase Discontinuities: Generalized Laws of Reflection and Refraction. *Science* **2011**, *334*, 333–337.
- (20) Cardano, F.; Marrucci, L. Spin–orbit photonics. *Nature Photonics* **2015**, *9*, 776–778.
- (21) Valev, V. K.; Baumberg, J. J.; Sibilia, C.; Verbiest, T. Chirality and Chiroptical Effects in Plasmonic Nanostructures: Fundamentals, Recent Progress, and Outlook. *Advanced Materials* **2013**, *25*, 2517–2534.
- (22) Falcone, F.; Lopetegi, T.; Laso, M. A. G.; Baena, J. D.; Bonache, J.; Beruete, M.; Marqués, R.; Martín, F.; Sorolla, M. Babinet Principle Applied to the Design of Metasurfaces and Metamaterials. *Physical Review Letters* **2004**, *93*, 197401.
- (23) Zentgraf, T.; Meyrath, T. P.; Seidel, A.; Kaiser, S.; Giessen, H.; Rockstuhl, C.; Lederer, F. Babinet’s principle for optical frequency metamaterials and nanoantennas. *Physical Review B* **2007**, *76*, 033407.
- (24) Horák, M.; Křápek, V.; Hrtoň, M.; Konečná, A.; Ligmajer, F.; Stöger-Pollach, M.; Šamořil, T.; Paták, A.; Édes, Z.; Metelka, O. et al. Limits of Babinet’s principle for solid and hollow plasmonic antennas. *Scientific Reports* **2019**, *9*, 4004.

- (25) Ligmajer, F.; Horák, M.; Šikola, T.; Fojta, M.; Daňhel, A. Silver Amalgam Nanoparticles and Microparticles: A Novel Plasmonic Platform for Spectroelectrochemistry. *The Journal of Physical Chemistry C* **2019**, *123*, 16957–16964.
- (26) Lei, D. Y.; Appavoo, K.; Ligmajer, F.; Sonnefraud, Y.; Haglund, R. F.; Maier, S. A. Optically-Triggered Nanoscale Memory Effect in a Hybrid Plasmonic-Phase Changing Nanostructure. *ACS Photonics* **2015**, *2*, 1306–1313.
- (27) Kepič, P.; Ligmajer, F.; Hrtoň, M.; Ren, H.; Menezes, L. d. S.; Maier, S. A.; Šikola, T. Optically Tunable Mie Resonance VO₂ Nanoantennas for Metasurfaces in the Visible. *ACS Photonics* **2021**, *8*, 1048–1057.
- (28) Liao, Y.; Fan, Y.; Lei, D. Thermally tunable binary-phase VO₂ metasurfaces for switchable holography and digital encryption. *Nanophotonics* **2024**, *13*, 1109–1117.
- (29) Kepič, P.; Horák, M.; Kabát, J.; Hájek, M.; Konečná, A.; Šikola, T.; Ligmajer, F. Coexisting Phases of Individual VO₂ Nanoparticles for Multilevel Nanoscale Memory. *ACS Nano* **2025**, *19*, 1167–1176.
- (30) Gutiérrez, Y.; Losurdo, M.; García-Fernández, P.; Sainz de la Maza, M.; González, F.; Brown, A. S.; Everitt, H. O.; Junquera, J.; Moreno, F. Gallium Polymorphs: Phase-Dependent Plasmonics. *Advanced Optical Materials* **2019**, *7*, 1900307.
- (31) Gutiérrez, Y.; García-Fernández, P.; Junquera, J.; Brown, A. S.; Moreno, F.; Losurdo, M. Polymorphic gallium for active resonance tuning in photonic nanostructures: from bulk gallium to two-dimensional (2D) gallene. *Nanophotonics* **2020**, *9*, 4233–4252.
- (32) Roy, P.; Bolshakov, A. D. Temperature-controlled switching of plasmonic response in gallium core-shell nanoparticles. *Journal of Physics D: Applied Physics* **2020**, *53*, 465303.

- (33) Xu, W.; Ling, X.; Xiao, J.; Dresselhaus, M. S.; Kong, J.; Xu, H.; Liu, Z.; Zhang, J. Surface enhanced Raman spectroscopy on a flat graphene surface. *Proceedings of the National Academy of Sciences* **2012**, *109*, 9281–9286.
- (34) Hartman, T.; Wondergem, C. S.; Kumar, N.; van den Berg, A.; Weckhuysen, B. M. Surface- and Tip-Enhanced Raman Spectroscopy in Catalysis. *The Journal of Physical Chemistry Letters* **2016**, *7*, 1570–1584.
- (35) Sanz, J. M.; Ortiz, D.; Alcaraz de la Osa, R.; Saiz, J. M.; González, F.; Brown, A. S.; Losurdo, M.; Everitt, H. O.; Moreno, F. UV Plasmonic Behavior of Various Metal Nanoparticles in the Near- and Far-Field Regimes: Geometry and Substrate Effects. *The Journal of Physical Chemistry C* **2013**, *117*, 19606–19615.
- (36) Knight, M. W.; King, N. S.; Liu, L.; Everitt, H. O.; Nordlander, P.; Halas, N. J. Aluminum for Plasmonics. *ACS Nano* **2013**, *8*, 834–840.
- (37) Toudert, J.; Serna, R.; Jiménez de Castro, M. Exploring the Optical Potential of Nano-Bismuth: Tunable Surface Plasmon Resonances in the Near Ultraviolet-to-Near Infrared Range. *The Journal of Physical Chemistry C* **2012**, *116*, 20530–20539.
- (38) Foltýn, M.; Kvapil, M.; Šikola, T.; Horák, M. Plasmonic Properties of Individual Bismuth Nanoparticles. *The Journal of Physical Chemistry Letters* **2025**, 9933–9938.
- (39) Knight, M. W.; Coenen, T.; Yang, Y.; Brenny, B. J. M.; Losurdo, M.; Brown, A. S.; Everitt, H. O.; Polman, A. Gallium Plasmonics: Deep Subwavelength Spectroscopic Imaging of Single and Interacting Gallium Nanoparticles. *ACS Nano* **2015**, *9*, 2049–2060.
- (40) Horák, M.; Čalkovský, V.; Mach, J.; Křápek, V.; Šikola, T. Plasmonic Properties of Individual Gallium Nanoparticles. *The Journal of Physical Chemistry Letters* **2023**, *14*, 2012–2019.

- (41) Horák, M.; Foltýn, M.; Čalkovský, V.; Mikerásek, V.; Bartošík, M.; Mach, J.; Šíkola, T. Plasmonic Response to Liquid–Solid Phase Transition in Individual Gallium Nanoparticles. *The Journal of Physical Chemistry Letters* **2025**, *16*, 8891–8896.
- (42) Biggins, J. S.; Yazdi, S.; Ringe, E. Magnesium Nanoparticle Plasmonics. *Nano Letters* **2018**, *18*, 3752–3758.
- (43) McMahon, J. M.; Schatz, G. C.; Gray, S. K. Plasmonics in the ultraviolet with the poor metals Al, Ga, In, Sn, Tl, Pb, and Bi. *Physical Chemistry Chemical Physics* **2013**, *15*, 5415–5423.
- (44) McMahon, J. M.; Schatz, G. C.; Gray, S. K. Correction: Plasmonics in the ultraviolet with the poor metals Al, Ga, In, Sn, Tl, Pb, and Bi. *Physical Chemistry Chemical Physics* **2015**, *17*, 19670–19671.
- (45) Hejazi, S. A.; Zaheer, Z.; Kosa, S. A. Plasmonic osmium hydrosols: Preparation, characterization, and properties. *Journal of Saudi Chemical Society* **2023**, *27*, 101651.
- (46) King, S. M.; Claire, S.; Teixeira, R. I.; Dosumu, A. N.; Carrod, A. J.; Dehghani, H.; Hannon, M. J.; Ward, A. D.; Bicknell, R.; Botchway, S. W. et al. Iridium Nanoparticles for Multichannel Luminescence Lifetime Imaging, Mapping Localization in Live Cancer Cells. *Journal of the American Chemical Society* **2018**, *140*, 10242–10249.
- (47) Chang, X.; Wang, Y.-F.; Zhang, X.; Wang, R.; Liu, Z.; Fu, J.; Zhao, D.; Li, F.; Wang, J.; Wang, W. et al. Iridium size effects in localized surface plasmon-enhanced diamond UV photodetectors. *Applied Surface Science* **2019**, *487*, 674–677.
- (48) Polyanskiy, M. N. Refractiveindex.info database of optical constants. *Scientific Data* **2024**, *11*, 94.
- (49) Rakić, A. D. Algorithm for the determination of intrinsic optical constants of metal films: application to aluminum. *Applied Optics* **1995**, *34*, 4755.

- (50) Werner, W. S. M.; Glantschnig, K.; Ambrosch-Draxl, C. Optical Constants and Inelastic Electron-Scattering Data for 17 Elemental Metals. *Journal of Physical and Chemical Reference Data* **2009**, *38*, 1013–1092.
- (51) Babar, S.; Weaver, J. H. Optical constants of Cu, Ag, and Au revisited. *Applied Optics* **2015**, *54*, 477.
- (52) Hagemann, H.-J.; Gudat, W.; Kunz, C. Optical constants from the far infrared to the x-ray region: Mg, Al, Cu, Ag, Au, Bi, C, and Al₂O₃. *Journal of the Optical Society of America* **1975**, *65*, 742.
- (53) Palik, E. D. *Handbook of Optical Constants of Solids*; Elsevier, 1985.
- (54) McPeak, K. M.; Jayanti, S. V.; Kress, S. J. P.; Meyer, S.; Iotti, S.; Rossinelli, A.; Norris, D. J. Plasmonic Films Can Easily Be Better: Rules and Recipes. *ACS Photonics* **2015**, *2*, 326–333.
- (55) Knight, M. W.; Liu, L.; Wang, Y.; Brown, L.; Mukherjee, S.; King, N. S.; Everitt, H. O.; Nordlander, P.; Halas, N. J. Aluminum Plasmonic Nanoantennas. *Nano Letters* **2012**, *12*, 6000–6004.
- (56) Clark, B. D.; Jacobson, C. R.; Lou, M.; Renard, D.; Wu, G.; Bursi, L.; Ali, A. S.; Swearer, D. F.; Tsai, A.-L.; Nordlander, P. et al. Aluminum Nanocubes Have Sharp Corners. *ACS Nano* **2019**, *13*, 9682–9691.
- (57) Langhammer, C.; Schwind, M.; Kasemo, B.; Zorić, I. Localized Surface Plasmon Resonances in Aluminum Nanodisks. *Nano Letters* **2008**, *8*, 1461–1471.
- (58) Schwind, M.; Kasemo, B.; Zorić, I. Localized and Propagating Plasmons in Metal Films with Nanoholes. *Nano Letters* **2013**, *13*, 1743–1750.
- (59) Martin, J.; Plain, J. Fabrication of aluminium nanostructures for plasmonics. *Journal of Physics D: Applied Physics* **2014**, *48*, 184002.

- (60) Clark, B. D.; Jacobson, C. R.; Lou, M.; Yang, J.; Zhou, L.; Gottheim, S.; DeSantis, C. J.; Nordlander, P.; Halas, N. J. Aluminum Nanorods. *Nano Letters* **2018**, *18*, 1234–1240.
- (61) Tan, S. J.; Zhang, L.; Zhu, D.; Goh, X. M.; Wang, Y. M.; Kumar, K.; Qiu, C.-W.; Yang, J. K. W. Plasmonic Color Palettes for Photorealistic Printing with Aluminum Nanostructures. *Nano Letters* **2014**, *14*, 4023–4029.
- (62) Douglas-Gallardo, O. A.; Soldano, G. J.; Mariscal, M. M.; Sánchez, C. G. Effects of oxidation on the plasmonic properties of aluminum nanoclusters. *Nanoscale* **2017**, *9*, 17471–17480.
- (63) Barulin, A.; Claude, J.-B.; Patra, S.; Moreau, A.; Lumeau, J.; Wenger, J. Preventing Aluminum Photocorrosion for Ultraviolet Plasmonics. *The Journal of Physical Chemistry Letters* **2019**, *10*, 5700–5707.
- (64) Li, L.; Fang Lim, S.; Poretzky, A. A.; Riehn, R.; Hallen, H. D. Near-field enhanced ultraviolet resonance Raman spectroscopy using aluminum bow-tie nano-antenna. *Applied Physics Letters* **2012**, *101*, 113116.
- (65) Akbay, N.; Lakowicz, J. R.; Ray, K. Distance-Dependent Metal-Enhanced Intrinsic Fluorescence of Proteins Using Polyelectrolyte Layer-by-Layer Assembly and Aluminum Nanoparticles. *The Journal of Physical Chemistry C* **2012**, *116*, 10766–10773.
- (66) Ray, K.; Szmackinski, H.; Lakowicz, J. R. Enhanced Fluorescence of Proteins and Label-Free Bioassays Using Aluminum Nanostructures. *Analytical Chemistry* **2009**, *81*, 6049–6054.
- (67) Najem, M.; Carcenac, F.; Coutaud, L.; Mouhibi, M.; Taliercio, T.; Gonzalez-Posada, F. Honeycomb-like aluminum antennas for surface-enhanced infrared absorption sensing. *Nanophotonics* **2023**, *12*, 2199–2212.

- (68) Canalejas-Tejero, V.; Herranz, S.; Bellingham, A.; Moreno-Bondi, M. C.; Barrios, C. A. Passivated Aluminum Nanohole Arrays for Label-Free Biosensing Applications. *ACS Applied Materials & Interfaces* **2013**, *6*, 1005–1010.
- (69) Zhou, X.; Gossage, Z. T.; Simpson, B. H.; Hui, J.; Barton, Z. J.; Rodríguez-López, J. Electrochemical Imaging of Photoanodic Water Oxidation Enhancements on TiO₂ Thin Films Modified by Subsurface Aluminum Nanodimers. *ACS Nano* **2016**, *10*, 9346–9352.
- (70) Liu, J.; Xu, M.; Zhang, T.; Chu, X.; Shi, K.; Li, J. Al/TiO₂ composite as a photocatalyst for the degradation of organic pollutants. *Environmental Science and Pollution Research* **2022**, *30*, 9738–9748.
- (71) Zhou, L.; Zhang, C.; McClain, M. J.; Manjavacas, A.; Krauter, C. M.; Tian, S.; Berg, F.; Everitt, H. O.; Carter, E. A.; Nordlander, P. et al. Aluminum Nanocrystals as a Plasmonic Photocatalyst for Hydrogen Dissociation. *Nano Letters* **2016**, *16*, 1478–1484.
- (72) Wang, C.; Yang, W.-C. D.; Raciti, D.; Bruma, A.; Marx, R.; Agrawal, A.; Sharma, R. Endothermic reaction at room temperature enabled by deep-ultraviolet plasmons. *Nature Materials* **2020**, *20*, 346–352.
- (73) Dogel, S.; Nattland, D.; Freyland, W. Complete wetting transitions at the liquid-vapor interface of gallium-bismuth alloys: Single-wavelength and spectroscopic ellipsometry studies. *Physical Review B* **2005**, *72*, 085403.
- (74) Foltýn, M.; Šikola, T.; Horák, M. Bismuth Plasmonic Antennas. *ACS Nano* **2025**, *19*, 32299–32305.
- (75) Sano, Y.; Satoh, H.; Chiba, M.; Shinohara, A.; Okamoto, M.; Serizawa, K.; Nakashima, H.; Omae, K. A 13-Week Toxicity Study of Bismuth in Rats by Intratracheal Intermittent Administration. *Journal of Occupational Health* **2005**, *47*, 242–248.

- (76) Griffith, D. M.; Li, H.; Werrett, M. V.; Andrews, P. C.; Sun, H. Medicinal chemistry and biomedical applications of bismuth-based compounds and nanoparticles. *Chemical Society Reviews* **2021**, *50*, 12037–12069.
- (77) Behnia, K.; Méasson, M.-A.; Kopelevich, Y. Nernst Effect in Semimetals: The Effective Mass and the Figure of Merit. *Physical Review Letters* **2007**, *98*, 076603.
- (78) Tian, Y.; Toudert, J. Nanobismuth: Fabrication, Optical, and Plasmonic Properties—Emerging Applications. *Journal of Nanotechnology* **2018**, *2018*, 1–23.
- (79) Wang, Y. W.; Kim, J. S.; Kim, G. H.; Kim, K. S. Quantum size effects in the volume plasmon excitation of bismuth nanoparticles investigated by electron energy loss spectroscopy. *Applied Physics Letters* **2006**, *88*, 143106.
- (80) Lee, S.; Ham, J.; Jeon, K.; Noh, J.-S.; Lee, W. Direct observation of the semimetal-to-semiconductor transition of individual single-crystal bismuth nanowires grown by on-film formation of nanowires. *Nanotechnology* **2010**, *21*, 405701.
- (81) Martínez-Lara, D.; González-Campuzano, R.; Mendoza, D. Quantum confinement effect in thin bismuth films: In search of the critical thickness for the semimetal–semiconductor transition. *Thin Solid Films* **2025**, *821*, 140678.
- (82) Son, J. S.; Park, K.; Han, M.; Kang, C.; Park, S.; Kim, J.; Kim, W.; Kim, S.; Hyeon, T. Large-Scale Synthesis and Characterization of the Size-Dependent Thermoelectric Properties of Uniformly Sized Bismuth Nanocrystals. *Angewandte Chemie International Edition* **2010**, *50*, 1363–1366.
- (83) Tarighatnia, A.; Fouladi, M. R.; Tohidkia, M. R.; Johal, G.; Nader, N. D.; Aghanejad, A.; Ghadiri, H. Engineering and quantification of bismuth nanoparticles as targeted contrast agent for computed tomography imaging in cellular and animal models. *Journal of Drug Delivery Science and Technology* **2021**, *66*, 102895.

- (84) Torrisi, L.; Silipigni, L.; Restuccia, N.; Cuzzocrea, S.; Cutroneo, M.; Barreca, F.; Fazio, B.; Di Marco, G.; Guglielmino, S. Laser-generated bismuth nanoparticles for applications in imaging and radiotherapy. *Journal of Physics and Chemistry of Solids* **2018**, *119*, 62–70.
- (85) Yang, C.; Guo, C.; Guo, W.; Zhao, X.; Liu, S.; Han, X. Multifunctional Bismuth Nanoparticles as Theranostic Agent for PA/CT Imaging and NIR Laser-Driven Photothermal Therapy. *ACS Applied Nano Materials* **2018**, *1*, 820–830.
- (86) Jiang, S.; Zhang, Y.; Gong, J. Applications of bismuth-based nanoparticles for the removal of pollutants in wastewater: a review. *Environmental Science: Nano* **2024**, *11*, 1332–1367.
- (87) Jia, G.; Wang, Y.; Sun, M.; Zhang, H.; Li, L.; Shi, Y.; Zhang, L.; Cui, X.; Lo, T. W. B.; Huang, B. et al. Size Effects of Highly Dispersed Bismuth Nanoparticles on Electrocatalytic Reduction of Carbon Dioxide to Formic Acid. *Journal of the American Chemical Society* **2023**, *145*, 14133–14142.
- (88) Dong, F.; Xiong, T.; Sun, Y.; Zhao, Z.; Zhou, Y.; Feng, X.; Wu, Z. A semimetal bismuth element as a direct plasmonic photocatalyst. *Chem. Commun.* **2014**, *50*, 10386–10389.
- (89) Qian, H.; Liu, Y.; Chen, H.; Feng, K.; Jia, K.; Pan, K.; Wang, G.; Huang, T.; Pang, X.; Zhang, Q. Emerging bismuth-based materials: From fundamentals to electrochemical energy storage applications. *Energy Storage Materials* **2023**, *58*, 232–270.
- (90) Leng, D.; Wang, T.; Li, Y.; Huang, Z.; Wang, H.; Wan, Y.; Pei, X.; Wang, J. Plasmonic Bismuth Nanoparticles: Thiolate Pyrolysis Synthesis, Size-Dependent LSPR Property, and Their Oxidation Behavior. *Inorganic Chemistry* **2021**, *60*, 17258–17267.
- (91) Martínez-Lara, D.; González-Campuzano, R.; Mendoza, D. Bismuth plasmonics in the

- visible spectrum using texturized films. *Photonics and Nanostructures - Fundamentals and Applications* **2022**, *52*, 101058.
- (92) Ozbay, I.; Ghobadi, A.; Butun, B.; Turhan-Sayan, G. Bismuth plasmonics for extraordinary light absorption in deep sub-wavelength geometries. *Optics Letters* **2020**, *45*, 686.
- (93) Chacon-Sanchez, F.; de Galarreta, C. R.; Nieto-Pinero, E.; Garcia-Pardo, M.; Garcia-Tabares, E.; Ramos, N.; Castillo, M.; Lopez-Garcia, M.; Siegel, J.; Toudert, J. et al. Building Conventional Metasurfaces with Unconventional Interband Plasmonics: A Versatile Route for Sustainable Structural Color Generation Based on Bismuth. *Advanced Optical Materials* **2024**, *12*, 2302130.
- (94) Sander, M. S.; Gronsky, R.; Lin, Y. M.; Dresselhaus, M. S. Plasmon excitation modes in nanowire arrays. *Journal of Applied Physics* **2001**, *89*, 2733–2736.
- (95) García de Abajo, F. J.; Howie, A. Retarded field calculation of electron energy loss in inhomogeneous dielectrics. *Physical Review B* **2002**, *65*, 115418.
- (96) Zhou, Y.; Li, W.; Zhang, Q.; Yan, S.; Cao, Y.; Dong, F.; Wang, F. Non-noble metal plasmonic photocatalysis in semimetal bismuth films for photocatalytic NO oxidation. *Phys. Chem. Chem. Phys.* **2017**, *19*, 25610–25616.
- (97) Johnson, P. B.; Christy, R. W. Optical Constants of the Noble Metals. *Physical Review B* **1972**, *6*, 4370–4379.
- (98) Jeong, S.; Liu, Y.; Zhong, Y.; Zhan, X.; Li, Y.; Wang, Y.; Cha, P. M.; Chen, J.; Ye, X. Heterometallic Seed-Mediated Growth of Monodisperse Colloidal Copper Nanorods with Widely Tunable Plasmonic Resonances. *Nano Letters* **2020**, *20*, 7263–7271.
- (99) Wang, P.; Yuan, Y.; Xu, K.; Zhong, H.; Yang, Y.; Jin, S.; Yang, K.; Qi, X. Biological applications of copper-containing materials. *Bioactive Materials* **2021**, *6*, 916–927.

- (100) Preston, A. S.; Hughes, R. A.; Demille, T. B.; Neretina, S. Plasmonics under Attack: Protecting Copper Nanostructures from Harsh Environments. *Chemistry of Materials* **2020**, *32*, 6788–6799.
- (101) Pramanick, B.; Upadhyay, B. Engineering the plasmonic activities of copper nanostructures for SERS and photocatalysis. *Applied Surface Science* **2025**, *682*, 161640.
- (102) Guo, H.; Chen, Y.; Cortie, M. B.; Liu, X.; Xie, Q.; Wang, X.; Peng, D.-L. Shape-Selective Formation of Monodisperse Copper Nanospheres and Nanocubes via Disproportionation Reaction Route and Their Optical Properties. *The Journal of Physical Chemistry C* **2014**, *118*, 9801–9808.
- (103) Lyu, Z.; Shang, Y.; Xia, Y. Shape-Controlled Synthesis of Copper Nanocrystals for Plasmonic, Biomedical, and Electrocatalytic Applications. *Accounts of Materials Research* **2022**, *3*, 1137–1148.
- (104) Adams, B. J.; Brown, E. M.; Phillips, W. T.; DuChene, J. S. Plasmon-Driven Synthesis of Cu Nanostructures. *Nano Letters* **2025**, *25*, 10218–10224.
- (105) Lu, S.-C.; Hsiao, M.-C.; Yorulmaz, M.; Wang, L.-Y.; Yang, P.-Y.; Link, S.; Chang, W.-S.; Tuan, H.-Y. Single-Crystalline Copper Nano-Octahedra. *Chemistry of Materials* **2015**, *27*, 8185–8188.
- (106) Chan, G. H.; Zhao, J.; Hicks, E. M.; Schatz, G. C.; Van Duyne, R. P. Plasmonic Properties of Copper Nanoparticles Fabricated by Nanosphere Lithography. *Nano Letters* **2007**, *7*, 1947–1952.
- (107) Mkhitarian, V.; March, K.; Tseng, E. N.; Li, X.; Scarabelli, L.; Liz-Marzán, L. M.; Chen, S.-Y.; Tizei, L. H. G.; Stéphan, O.; Song, J.-M. et al. Can Copper Nanostructures Sustain High-Quality Plasmons? *Nano Letters* **2021**, *21*, 2444–2452.

- (108) Gu, Z.; Shen, H.; Shang, L.; Lv, X.; Qian, L.; Zheng, G. Nanostructured Copper-Based Electrocatalysts for CO₂ Reduction. *Small Methods* **2018**, *2*, 1800121.
- (109) Johnson, R. C.; Li, J.; Hupp, J. T.; Schatz, G. C. Hyper-Rayleigh scattering studies of silver, copper, and platinum nanoparticle suspensions. *Chemical Physics Letters* **2002**, *356*, 534–540.
- (110) Sun, Q.-C.; Ding, Y.; Goodman, S. M.; H. Funke, H.; Nagpal, P. Copper plasmonics and catalysis: role of electron–phonon interactions in dephasing localized surface plasmons. *Nanoscale* **2014**, *6*, 12450–12457.
- (111) Tyagi, S.; Kashyap, R. K.; Dhankhar, A.; Pillai, P. P. Plasmon-powered chemistry with visible-light active copper nanoparticles. *Chemical Science* **2024**, *15*, 16997–17006.
- (112) Simayee, M.; Iraji zad, A.; Esfandiar, A. Green synthesise of copper nanoparticles on the cotton fabric as a self-regenerating and high-efficient plasmonic solar evaporator. *Scientific Reports* **2023**, *13*, 12762.
- (113) Huang, C.-L.; Kumar, G.; Sharma, G. D.; Chen, F.-C. Plasmonic effects of copper nanoparticles in polymer photovoltaic devices for outdoor and indoor applications. *Applied Physics Letters* **2020**, *116*, 253302.
- (114) Gloystein, A.; Nilius, N. Copper oxide phases probed via plasmonic light emission in the STM. *New Journal of Physics* **2021**, *23*, 093021.
- (115) Yaremchuk, I.; Bulavinets, T. Study of plasmonic properties of copper monosulfide nanoparticles depending on their dielectric constant. *Technology audit and production reserves* **2021**, *4*, 9–13.
- (116) Chitambar, C. R. Medical Applications and Toxicities of Gallium Compounds. *International Journal of Environmental Research and Public Health* **2010**, *7*, 2337–2361.

- (117) Yu, H.-S.; Liao, W.-T. *Encyclopedia of Environmental Health*; Elsevier, 2011; p 829–833.
- (118) Li, R.; Wang, L.; Li, L.; Yu, T.; Zhao, H.; Chapman, K. W.; Wang, Y.; Rivers, M. L.; Chupas, P. J.; Mao, H.-k. et al. Local structure of liquid gallium under pressure. *Scientific Reports* **2017**, *7*, 5666.
- (119) Gutiérrez, Y.; Losurdo, M.; García-Fernández, P.; Sainz de la Maza, M.; González, F.; Brown, A. S.; Everitt, H. O.; Junquera, J.; Moreno, F. Dielectric function and plasmonic behavior of Ga(II) and Ga(III). *Optical Materials Express* **2019**, *9*, 4050.
- (120) Yarema, M.; Wörle, M.; Rossell, M. D.; Erni, R.; Caputo, R.; Protesescu, L.; Kravchyk, K. V.; Dirin, D. N.; Lienau, K.; von Rohr, F. et al. Monodisperse Colloidal Gallium Nanoparticles: Synthesis, Low Temperature Crystallization, Surface Plasmon Resonance and Li-Ion Storage. *Journal of the American Chemical Society* **2014**, *136*, 12422–12430.
- (121) Schenk, F. M.; Wintersteller, S.; Clarysse, J.; He, H.; von Mentlen, J.-M.; Yazdani, N.; Wied, M.; Wood, V.; Prehal, C.; Yarema, M. Rational Design for Monodisperse Gallium Nanoparticles by In Situ Monitoring with Small-Angle X-ray Scattering. *Journal of the American Chemical Society* **2025**, *147*, 12105–12114.
- (122) MacDonald, K. F.; Fedotov, V. A.; Pochon, S.; Ross, K. J.; Stevens, G. C.; Zheludev, N. I.; Brocklesby, W. S.; Emel'yanov, V. I. Optical control of gallium nanoparticle growth. *Applied Physics Letters* **2002**, *80*, 1643–1645.
- (123) Wu, P. C.; Kim, T.-H.; Brown, A. S.; Losurdo, M.; Bruno, G.; Everitt, H. O. Real-time plasmon resonance tuning of liquid Ga nanoparticles by in situ spectroscopic ellipsometry. *Applied Physics Letters* **2007**, *90*, 103119.
- (124) Kolíbal, M.; Čechal, T.; Brandejsová, E.; Čechal, J.; Šíkola, T. Self-limiting cyclic growth of gallium droplets on Si(111). *Nanotechnology* **2008**, *19*, 475606.

- (125) Catalán-Gómez, S.; Bran, C.; Vázquez, M.; Vázquez, L.; Pau, J. L.; Redondo-Cubero, A. Plasmonic coupling in closed-packed ordered gallium nanoparticles. *Scientific Reports* **2020**, *10*, 4187.
- (126) Di Cicco, A. Phase Transitions in Confined Gallium Droplets. *Physical Review Letters* **1998**, *81*, 2942–2945.
- (127) de la Mata, M.; Catalán-Gómez, S.; Nucciarelli, F.; Pau, J. L.; Molina, S. I. High Spatial Resolution Mapping of Localized Surface Plasmon Resonances in Single Gallium Nanoparticles. *Small* **2019**, *15*, 1902920.
- (128) Ma, H.; Tian, Y.; Jiao, A.; Wang, C.; Zhang, M.; Zheng, L.; Li, G.; Li, S.; Chen, M. Extraordinary approach to further boost plasmonic NIR-SERS by cryogenic temperature-suppressed non-radiative recombination. *Optics Letters* **2022**, *47*, 670.
- (129) Xu, L.; Chen, M.; Cui, Q.; Wang, C.; Zhang, M.; Zheng, L.; Li, S.; Zhang, H.; Liang, G. Ultra-clean ternary Au/Ag/AgCl nanoclusters favoring cryogenic temperature-boosted broadband SERS ultrasensitive detection. *Optics Express* **2023**, *31*, 26474.
- (130) Catalán-Gómez, S.; Redondo-Cubero, A.; Palomares, F. J.; Nucciarelli, F.; Pau, J. L. Tunable plasmonic resonance of gallium nanoparticles by thermal oxidation at low temperatures. *Nanotechnology* **2017**, *28*, 405705.
- (131) Catalán-Gómez, S.; Redondo-Cubero, A.; Palomares, F. J.; Vázquez, L.; Nogales, E.; Nucciarelli, F.; Méndez, B.; Gordillo, N.; Pau, J. L. Size-selective breaking of the core-shell structure of gallium nanoparticles. *Nanotechnology* **2018**, *29*, 355707.
- (132) Reineck, P.; Lin, Y.; Gibson, B. C.; Dickey, M. D.; Greentree, A. D.; Maksymov, I. S. UV plasmonic properties of colloidal liquid-metal eutectic gallium-indium alloy nanoparticles. *Scientific Reports* **2019**, *9*, 5345.

- (133) Lereu, A. L.; Lemarchand, F.; Zerrad, M.; Yazdanpanah, M.; Passian, A. Optical properties and plasmonic response of silver-gallium nanostructures. *Journal of Applied Physics* **2015**, *117*, 063110.
- (134) Marín, A. G.; García-Mendiola, T.; Bernabeu, C. N.; Hernández, M. J.; Piqueras, J.; Pau, J. L.; Pariente, F.; Lorenzo, E. Gallium plasmonic nanoparticles for label-free DNA and single nucleotide polymorphism sensing. *Nanoscale* **2016**, *8*, 9842–9851.
- (135) Catalán-Gómez, S.; Garg, S.; Redondo-Cubero, A.; Gordillo, N.; de Andrés, A.; Nucciarelli, F.; Kim, S.; Kung, P.; Pau, J. L. Photoluminescence enhancement of monolayer MoS₂ using plasmonic gallium nanoparticles. *Nanoscale Advances* **2019**, *1*, 884–893.
- (136) Wu, P. C.; Khoury, C. G.; Kim, T.-H.; Yang, Y.; Losurdo, M.; Bianco, G. V.; Vo-Dinh, T.; Brown, A. S.; Everitt, H. O. Demonstration of Surface-Enhanced Raman Scattering by Tunable, Plasmonic Gallium Nanoparticles. *Journal of the American Chemical Society* **2009**, *131*, 12032–12033.
- (137) Yang, Y.; Callahan, J. M.; Kim, T.-H.; Brown, A. S.; Everitt, H. O. Ultraviolet Nanoplasmonics: A Demonstration of Surface-Enhanced Raman Spectroscopy, Fluorescence, and Photodegradation Using Gallium Nanoparticles. *Nano Letters* **2013**, *13*, 2837–2841.
- (138) Dumiszewska, E.; Caban, P.; Józwiak, I.; Ciepielewski, P.; Baranowski, J. M. MOCVD growth of gallium and indium microparticles for SERS applications. *Journal of Materials Science: Materials in Electronics* **2021**, *32*, 8958–8964.
- (139) Piastek, J.; Mach, J.; Bardy, S.; Édes, Z.; Bartošík, M.; Maniš, J.; Čalkovský, V.; Konečný, M.; Spousta, J.; Šikola, T. Correlative Raman Imaging and Scanning Electron Microscopy: The Role of Single Ga Islands in Surface-Enhanced Raman Spectroscopy of Graphene. *The Journal of Physical Chemistry C* **2022**, *126*, 4508–4514.

- (140) Palm, K. J.; Murray, J. B.; Narayan, T. C.; Munday, J. N. Dynamic Optical Properties of Metal Hydrides. *ACS Photonics* **2018**, *5*, 4677–4686.
- (141) Appusamy, K.; Blair, S.; Nahata, A.; Guruswamy, S. Low-loss magnesium films for plasmonics. *Materials Science and Engineering: B* **2014**, *181*, 77–85.
- (142) Sterl, F.; Strohfeldt, N.; Walter, R.; Griessen, R.; Tittl, A.; Giessen, H. Magnesium as Novel Material for Active Plasmonics in the Visible Wavelength Range. *Nano Letters* **2015**, *15*, 7949–7955.
- (143) Asselin, J.; Boukouvala, C.; Hopper, E. R.; Ramasse, Q. M.; Biggins, J. S.; Ringe, E. Tents, Chairs, Tacos, Kites, and Rods: Shapes and Plasmonic Properties of Singly Twinned Magnesium Nanoparticles. *ACS Nano* **2020**, *14*, 5968–5980.
- (144) Ringe, E. Shapes, Plasmonic Properties, and Reactivity of Magnesium Nanoparticles. *The Journal of Physical Chemistry C* **2020**, *124*, 15665–15679.
- (145) Pehlivan, Z. S.; Ten, A.; Wayman, T. M. R.; Ringe, E. Plasmonic magnesium arrays with nanosphere lithography. *APL Photonics* **2024**, *9*, 071302.
- (146) Asselin, J.; Hopper, E. R.; Ringe, E. Improving the stability of plasmonic magnesium nanoparticles in aqueous media. *Nanoscale* **2021**, *13*, 20649–20656.
- (147) Ten, A.; Lomonosov, V.; Boukouvala, C.; Ringe, E. Magnesium Nanoparticles for Surface-Enhanced Raman Scattering and Plasmon-Driven Catalysis. *ACS Nano* **2024**, *18*, 18785–18799.
- (148) West, C. A.; Lomonosov, V.; Pehlivan, Z. S.; Ringe, E. Plasmonic Magnesium Nanoparticles Are Efficient Nanoheaters. *Nano Letters* **2023**, *23*, 10964–10970.
- (149) Liu, L.; Wu, Y.; Ye, J.; Fu, Q.; Su, L.; Wu, Z.; Feng, J.; Chen, Z.; Song, J. Synthesis of magnesium nanoparticle for NIR-II-photoacoustic-imaging-guided synergistic burst-like and H2 cancer therapy. *Chem* **2022**, *8*, 2990–3007.

- (150) Jeong, H.-H.; Mark, A. G.; Fischer, P. Magnesium plasmonics for UV applications and chiral sensing. *Chemical Communications* **2016**, *52*, 12179–12182.
- (151) Li, R.; Xie, S.; Zhang, L.; Li, L.; Kong, D.; Wang, Q.; Xin, R.; Sheng, X.; Yin, L.; Yu, C. et al. Soft and transient magnesium plasmonics for environmental and biomedical sensing. *Nano Research* **2018**, *11*, 4390–4400.
- (152) Lomonosov, V.; Wayman, T. M. R.; Hopper, E. R.; Ivanov, Y. P.; Divitini, G.; Ringe, E. Plasmonic magnesium nanoparticles decorated with palladium catalyze thermal and light-driven hydrogenation of acetylene. *Nanoscale* **2023**, *15*, 7420–7429.
- (153) Duan, X.; Liu, N. Magnesium for Dynamic Nanoplasmonics. *Accounts of Chemical Research* **2019**, *52*, 1979–1989.
- (154) Sterl, F.; Linnenbank, H.; Steinle, T.; Mörz, F.; Strohfeldt, N.; Giessen, H. Nanoscale Hydrogenography on Single Magnesium Nanoparticles. *Nano Letters* **2018**, *18*, 4293–4302.
- (155) Golovashkin, A.; Motulevich, G. Optical and Electrical Properties of Tin. *Journal of Experimental and Theoretical Physics (Soviet Physics)* **1964**, *19*, 310–317.
- (156) Petrakian, J. P.; Cathers, A. R.; Parks, J. E.; MacRae, R. A.; Callcott, T. A.; Arakawa, E. T. Optical properties of liquid tin between 0.62 and 3.7 eV. *Physical Review B* **1980**, *21*, 3043–3046.
- (157) Li, B.; Wu, H.-H.; Luo, P.-F.; Lin, K.; Cheng, J.-G.; Zhong, H.-H.; Jiang, Y.; Lu, Y.-W. Size-Dependent Plasmonic Mode Evolution and SERS Performance of β -Sn Nanoparticles. *The Journal of Physical Chemistry C* **2018**, *123*, 735–738.
- (158) He, X.; He, Y.; Sun, C. A Study of the Plasmonic Metasurface Based on Hexagonally Oriented Sn Nanobars. *Plasmonics* **2024**, *20*, 2861–2868.

- (159) Lai, S. L.; Guo, J. Y.; Petrova, V.; Ramanath, G.; Allen, L. H. Size-Dependent Melting Properties of Small Tin Particles: Nanocalorimetric Measurements. *Physical Review Letters* **1996**, *77*, 99–102.
- (160) Jo, Y. H.; Jung, I.; Choi, C. S.; Kim, I.; Lee, H. M. Synthesis and characterization of low temperature Sn nanoparticles for the fabrication of highly conductive ink. *Nanotechnology* **2011**, *22*, 225701.
- (161) Kryshstal, A.; Bogatyrenko, S.; Khshanovska, O. Direct Imaging of Surface Melting on a Single Sn Nanoparticle. *Nano Letters* **2023**, *23*, 6354–6359.
- (162) Schwind, M.; Zhdanov, V. P.; Zorić, I.; Kasemo, B. LSPR Study of the Kinetics of the Liquid-Solid Phase Transition in Sn Nanoparticles. *Nano Letters* **2010**, *10*, 931–936.
- (163) Kryshstal, A.; Khshanovska, O. Probing the local thermal expansion coefficient of single liquid Sn nanoparticles using EELS in STEM. *Scientific Reports* **2025**, *15*, 5335.
- (164) Molodets, A. M.; Nabatov, S. S. Thermodynamic potentials, diagram of state, and phase transitions of tin on shock compression. *High Temperature* **2000**, *38*, 715–721.
- (165) Johansen, B.; Uhrenfeldt, C.; Nylandsted Larsen, A. Plasmonic Properties of β -Sn Nanoparticles in Ordered and Disordered Arrangements. *Plasmonics* **2012**, *8*, 153–158.
- (166) Wohlwend, J.; Haberfehlner, G.; Galinski, H. Strong Coupling in Two-Phase Metamaterials Fabricated by Sequential Self-Assembly. *Advanced Optical Materials* **2023**, *11*, 2300568.
- (167) Minnai, C.; Vanzan, A.; Reidy, L. C.; LaGrow, A. P.; Di Vece, M. Visible Light Silver Nanoantenna on UV Responding Tin Nanoparticles. *Advanced Optical Materials* **2025**, *13*, 2403432.

- (168) Kjeldsen, M. M.; Hansen, J. L.; Pedersen, T. G.; Gaiduk, P.; Larsen, A. N. Tuning the plasmon resonance of metallic tin nanocrystals in Si-based materials. *Applied Physics A* **2010**, *100*, 31–37.
- (169) Minnai, C.; Vanzan, A.; Reidy, L. C.; LaGrow, A. P.; Di Vece, M. Begrenzung effect in Si₃N₄ encapsulated plasmonic Sn nanoparticles. *Physical Review B* **2024**, *110*, 205411.
- (170) Jung, J.; Pedersen, T. G.; Søndergaard, T.; Pedersen, K.; Larsen, A. N.; Nielsen, B. B. On localized surface plasmons of metallic tin nanoparticles in silicon. *physica status solidi (RRL) – Rapid Research Letters* **2010**, *4*, 292–294.
- (171) Chen, Y.; Wang, M.; Zheng, K.; Ren, Y.; Xu, H.; Yu, Z.; Zhou, F.; Liu, C.; Qu, J.; Song, J. Antimony Nanopolyhedrons with Tunable Localized Surface Plasmon Resonances for Highly Effective Photoacoustic-Imaging-Guided Synergistic Photothermal/Immunotherapy. *Advanced Materials* **2021**, *33*, 2100039.
- (172) Ghorai, G.; Ghosh, K.; Das, B.; Sahoo, S.; Patra, B.; Samal, P.; Sahoo, P. K. Cathodoluminescence and optical absorption spectroscopy of plasmonic modes in chromium micro-rods. *Nanotechnology* **2022**, *34*, 075707.
- (173) Karaballi, R. A.; Monfared, Y. E.; Bicket, I. C.; Coridan, R. H.; Dasog, M. Solid-state synthesis of UV-plasmonic Cr₂N nanoparticles. *The Journal of Chemical Physics* **2022**, *157*, 154706.
- (174) McKenna, H. D. L.; Shrestha, B.; Lu, E.; Lott, H.; Subedi, I.; Chen, X.; Hwang, S.; Zakharov, D.; Podraza, N. J.; Yang, J. C. et al. Formation and optical properties of indium nanoparticle arrays for deep-UV plasmonics. *Applied Physics Letters* **2025**, *127*, 031701.
- (175) Matsuda, R.; Yao, H. UV-resonant magnetoplasmonic properties of chemically syn-

- thesized indium nanoparticles. *Physical Chemistry Chemical Physics* **2024**, *26*, 8850–8857.
- (176) George, A.; Choudhary, H. K.; Satpati, B.; Mandal, S. Synthesis, characterization and optical properties of ligand-protected indium nanoparticles. *Physical Chemistry Chemical Physics* **2015**, *17*, 7109–7113.
- (177) Wang, L.; Guo, S.; Liu, D.; He, J.; Zhou, J.; Zhang, K.; Wei, Y.; Pan, Y.; Gao, C.; Yuan, Z. et al. Plasmon-Enhanced Blue Upconversion Luminescence by Indium Nanocrystals. *Advanced Functional Materials* **2019**, *29*, 1901242.
- (178) Ho, W.-J.; Yang, H.-Y.; Liu, J.-J.; Lin, P.-J.; Ho, C.-H. Plasmonic effects of two-dimensional indium-nanoparticles embedded within SiO₂ anti-reflective coating on the performance of silicon solar cells. *Applied Surface Science* **2020**, *508*, 145275.
- (179) Das, R.; Soni, R. K. Synthesis and surface-enhanced Raman scattering of indium nanotriangles and nanowires. *RSC Advances* **2017**, *7*, 32255–32263.
- (180) González-Campuzano, R.; Martínez-Lara, D. E.; Mendoza, D. Lead plasmonics on texturized substrates: Pb metafilms. *Applied Physics Letters* **2020**, *117*, 031603.
- (181) Wang, C.; Cui, T.; Liu, Z.; Lin, Y.; Tang, S.; Shao, L.; Chen, H.; Shen, Y.; Deng, S. Molybdenum Truncated Cone Arrays with Localized Surface Plasmon Resonance for Surface-Enhanced Raman Scattering Application. *Photonics* **2024**, *11*, 950.
- (182) Etman, A. S.; Wang, L.; Edström, K.; Nyholm, L.; Sun, J. Molybdenum Oxide Nanosheets with Tunable Plasmonic Resonance: Aqueous Exfoliation Synthesis and Charge Storage Applications. *Advanced Functional Materials* **2018**, *29*, 1806699.
- (183) Kong, W.; Liu, W.; Zheng, X.; Xu, Q. Sunlight Driven Reversible and Tunable Plasmon Resonance in 2D Amorphous Molybdenum Oxide. *Advanced Optical Materials* **2023**, *12*, 2301821.

- (184) Guan, H.; Yi, W.; Li, T.; Li, Y.; Li, J.; Bai, H.; Xi, G. Low temperature synthesis of plasmonic molybdenum nitride nanosheets for surface enhanced Raman scattering. *Nature Communications* **2020**, *11*, 3889.
- (185) Sharma, V.; Chotia, C.; Tarachand, T.; Ganesan, V.; Okram, G. S. Influence of particle size and dielectric environment on the dispersion behaviour and surface plasmon in nickel nanoparticles. *Physical Chemistry Chemical Physics* **2017**, *19*, 14096–14106.
- (186) Kataja, M.; Freire-Fernández, F.; Witteveen, J. P.; Hakala, T. K.; Törmä, P.; van Dijken, S. Plasmon-induced demagnetization and magnetic switching in nickel nanoparticle arrays. *Applied Physics Letters* **2018**, *112*, 072406.
- (187) Gao, Z.; Wildenborg, A.; Kocoj, C. A.; Liu, E.; Sheofsky, C.; Rawashdeh, A.; Qu, H.; Guo, P.; Suh, J. Y.; Yang, A. Low-Loss Plasmonics with Nanostructured Potassium and Sodium–Potassium Liquid Alloys. *Nano Letters* **2023**, *23*, 7150–7156.
- (188) Abadi, E. H. L.; Amiri, M.; Ranaee, M.; Mortazavi-Derazkola, S.; Khademian, A.; Najafzadehvarzi, H.; Ghoreishi, S. M. Plasmonic Selenium Nanoparticles Biosynthesized from *Crataegus monogyna* Fruit Extract: A Novel Approach to Mitigating Chromium-Induced Toxicity. *Plasmonics* **2024**, *20*, 3805–3815.
- (189) Rawashdeh, A.; Wildenborg, A.; Liu, E.; Gao, Z.; Czaplewski, D. A.; Qu, H.; Suh, J. Y.; Yang, A. High-Quality Surface Plasmon Polaritons in Large-Area Sodium Nanostructures. *Nano Letters* **2023**, *23*, 469–475.
- (190) Kocoj, C. A.; Xie, X.; Jiang, H.; Li, S.; Sarker, S.; Yang, A.; Guo, P. Ultrafast Plasmon Dynamics of Low-Loss Sodium Metasurfaces. *ACS Nano* **2025**, *19*, 27310–27317.
- (191) Ma, C.; Yan, J.; Huang, Y.; Wang, C.; Yang, G. The optical duality of tellurium nanoparticles for broadband solar energy harvesting and efficient photothermal conversion. *Science Advances* **2018**, *4*, eaas9894.

- (192) Naik, G. V.; Schroeder, J. L.; Ni, X.; Kildishev, A. V.; Sands, T. D.; Boltasseva, A. Titanium nitride as a plasmonic material for visible and near-infrared wavelengths. *Optical Materials Express* **2012**, *2*, 478.
- (193) Mahajan, U.; Dhonde, M.; Sahu, K.; Ghosh, P.; Shirage, P. M. Titanium nitride (TiN) as a promising alternative to plasmonic metals: a comprehensive review of synthesis and applications. *Materials Advances* **2024**, *5*, 846–895.
- (194) Zhu, L.; Gao, J.; Gu, W.; Zhang, F.; Geng, H.; Xu, J.; Liu, Z. Surface plasmon resonance of the W nanowires. *Materials Research Express* **2022**, *9*, 125005.
- (195) Lu, C.; Li, J.; Chen, G.; Li, B.; Lou, Z. Self-Z-scheme plasmonic tungsten oxide nanowires for boosting ethanol dehydrogenation under UV-visible light irradiation. *Nanoscale* **2019**, *11*, 12774–12780.
- (196) Davis Jr, G. A.; Wyatt, B. C.; Muhoberac, B. B.; Sardar, R. Unveiling the Effect of Shape Anisotropy of Plasmonic Tungsten Oxide Nanostructures for Enhanced Electrocatalytic Hydrogen Evolution. *Chemistry of Materials* **2025**, *37*, 610–623.
- (197) Tian, D.; Liu, X.; Li, J.; Wang, Z.; Cai, X.; Chen, J.; Jin, H.; Li, B.; Lou, Z. Constructing High-Active Surface of Plasmonic Tungsten Oxide for Photocatalytic Alcohol Dehydration. *Advanced Materials* **2024**, *36*, 2404738.
- (198) Amekura, H.; Umeda, N.; Kono, K.; Takeda, Y.; Kishimoto, N.; Buchal, C.; Mantl, S. Dual surface plasmon resonances in Zn nanoparticles in SiO₂: an experimental study based on optical absorption and thermal stability. *Nanotechnology* **2007**, *18*, 395707.
- (199) Amekura, H.; Shinotsuka, H.; Yoshikawa, H. Are the triple surface plasmon resonances in Zn nanoparticles true? *Nanotechnology* **2017**, *28*, 495712.
- (200) Tomaev, V. V.; Polishchuk, V. A.; Vartanyan, T. A.; Vasil'ev, E. A. Surface Plasmon Resonance in Zinc Nanoparticles. *Glass Physics and Chemistry* **2019**, *45*, 238–241.

- (201) Li, N.; Jiao, F.; Pan, X.; Ding, Y.; Feng, J.; Bao, X. Size Effects of ZnO Nanoparticles in Bifunctional Catalysts for Selective Syngas Conversion. *ACS Catalysis* **2018**, *9*, 960–966.
- (202) Kelly, S. R.; Shi, X.; Back, S.; Vallez, L.; Park, S. Y.; Siahrostami, S.; Zheng, X.; Nørskov, J. K. ZnO As an Active and Selective Catalyst for Electrochemical Water Oxidation to Hydrogen Peroxide. *ACS Catalysis* **2019**, *9*, 4593–4599.
- (203) Fageria, P.; Gangopadhyay, S.; Pande, S. Synthesis of ZnO/Au and ZnO/Ag nanoparticles and their photocatalytic application using UV and visible light. *RSC Adv.* **2014**, *4*, 24962–24972.
- (204) Song, S.; Song, H.; Li, L.; Wang, S.; Chu, W.; Peng, K.; Meng, X.; Wang, Q.; Deng, B.; Liu, Q. et al. A selective Au-ZnO/TiO₂ hybrid photocatalyst for oxidative coupling of methane to ethane with dioxygen. *Nature Catalysis* **2021**, *4*, 1032–1042.